LETTER

doi:10.1038/nature24993

Runx3 programs CD8$^+$ T cell residency in non-lymphoid tissues and tumours

J. Justin Milner[1], Clara Toma[1]*, Bingfei Yu[1]*, Kai Zhang[2], Kyla Omilusik[1], Anthony T. Phan[1], Dapeng Wang[3], Adam J. Getzler[3], Toan Nguyen[1], Shane Crotty[4,5], Wei Wang[2,6,7], Matthew E. Pipkin[3] & Ananda W. Goldrath[1]

Tissue-resident memory CD8$^+$ T (T_{RM}) cells are found at common sites of pathogen exposure, where they elicit rapid and robust protective immune responses[1,2]. However, the molecular signals that control T_{RM} cell differentiation and homeostasis are not fully understood. Here we show that mouse T_{RM} precursor cells represent a unique CD8$^+$ T cell subset that is distinct from the precursors of circulating memory cell populations at the levels of gene expression and chromatin accessibility. Using computational and pooled *in vivo* RNA interference screens, we identify the transcription factor Runx3 as a key regulator of T_{RM} cell differentiation and homeostasis. Runx3 was required to establish T_{RM} cell populations in diverse tissue environments, and supported the expression of crucial tissue-residency genes while suppressing genes associated with tissue egress and recirculation. Furthermore, we show that human and mouse tumour-infiltrating lymphocytes share a core tissue-residency gene-expression signature with T_{RM} cells that is associated with Runx3 activity. In a mouse model of adoptive T cell therapy for melanoma, *Runx3*-deficient CD8$^+$ tumour-infiltrating lymphocytes failed to accumulate in tumours, resulting in greater rates of tumour growth and mortality. Conversely, overexpression of Runx3 enhanced tumour-specific CD8$^+$ T cell abundance, delayed tumour growth, and prolonged survival. In addition to establishing Runx3 as a central regulator of T_{RM} cell differentiation, these results provide insight into the signals that promote T cell residency in non-lymphoid sites, which could be used to enhance vaccine efficacy or adoptive cell therapy treatments that target cancer.

Long-lived memory T cells provide protection from reinfection and can serve as endogenous defenders against tumour growth[3]. Memory CD8$^+$ T cell populations can be broadly segregated into circulating central memory (T_{CM}) and effector memory (T_{EM}) T cells as well as tissue-resident memory (T_{RM}) T cells that primarily reside in non-lymphoid tissues without egress[4]. Circulating memory CD8$^+$ T cells and T_{RM} cells exhibit distinct gene-expression profiles[5–7]; however, the early transcriptional identity of differentiating T_{RM} cells and the signals controlling their fate are not yet fully appreciated. Here, we used an established infection model with P14 T cell receptor transgenic CD8$^+$ T cells responsive to the lymphocytic choriomeningitis virus (LCMV) glycoprotein 33–41 peptide ($GP_{33–41}$) presented by major histocompatibility complex (MHC) class I H-2D^b. In this acute infection model, adoptively transferred P14 cells located in non-lymphoid tissues on day 7 of infection began to upregulate molecules characteristic of T_{RM} cells[8], including key tissue-retention molecules CD103 and CD69 (Extended Data Fig. 1a). Gene expression analysis revealed that 90–96% of the genes upregulated in mature P14 T_{RM} cells in the kidney parenchyma or intraepithelial lymphocyte (IEL) compartment of the small intestine were increased in T_{RM} precursor cells relative to splenic effector cells on day 7 of infection (Fig. 1a). Furthermore, analysis of genes differentially expressed between splenic and non-lymphoid populations on day 7 of infection revealed two distinct gene expression programs that segregated circulating (peripheral blood lymphocytes, spleen, T_{CM} and T_{EM}) from non-lymphoid (kidney and IELs) P14 cells, independent of the infection time point (Fig. 1b). Lymph node or splenic KLRG1^{lo}CD127^{hi} memory precursor cells preferentially give rise to circulating memory populations, whereas shorter-lived KLRG1^{hi}CD127^{lo} terminal effector cells exhibit less memory potential[3]. Day 7 IEL P14 cells comprising the precursors of T_{RM} cells were transcriptionally distinct from splenic memory precursor cells (Fig. 1c). This is notable, as IEL T_{RM} cells are predominantly KLRG1^{lo} (ref. 9) and preferentially differentiate from lymphoid-derived KLRG1^{lo} precursors seeding non-lymphoid tissues on days 4.5–7 of infection[10] (Extended Data Fig. 1a–c), consistent with studies of skin T_{RM} cells[5]. Thus, the T_{RM} precursor cell populations in non-lymphoid tissues are transcriptionally distinct from circulating effector cells as well as memory precursor cells on day 7 of infection, and most of the T_{RM} cell transcriptional program is already established at this time point, before contraction of the CD8$^+$ T cell population.

As chromatin accessibility is a key determinant of cell identity and fate, we profiled non-lymphoid and splenic effector populations using an assay for transposase-accessible chromatin with high-throughput sequencing (ATAC–seq) on day 7 of infection. Uniquely accessible chromatin regions were identified in IEL P14 cells near genes characteristically expressed in mature T_{RM} cells (for example, *Cd69* and *Nr4a1*), whereas genes that promote T cell re-circulation (for example, *Klf2* and *S1pr1*) exhibited loss of accessible regions (Extended Data Fig. 2a). Principal component analysis (PCA) highlighted that, despite day 7 being an 'effector' time point, the global chromatin landscape markedly differs between effector CD8$^+$ T cells located in the spleen, including memory precursor cells, and those located in non-lymphoid tissues (Fig. 1d). The unique chromatin configuration of differentiating T_{RM} cells is consistent with the notable transcriptional differences observed (Fig. 1a–c) and foreshadows the distinct fates of antigen-specific cells in the spleen relative to non-lymphoid tissues. Thus, precursors of T_{RM} cells in non-lymphoid sites are a unique and distinct CD8$^+$ T cell subset relative to effector cells in the lymphoid compartment, including the memory precursor cell population.

Specification of CD8$^+$ T cell fate during infection is dependent on the integrated activity of multiple transcription factors[3]; regulators of T_{RM} cell formation include Hobit[6], Blimp1[6], Nr4a1[11], Eomes[12] and T-bet[12,13]. To facilitate a broader understanding of the transcriptional network driving T_{RM} cell differentiation, we used a combined screening approach, consisting of a computational strategy integrating ATAC–seq data, transcriptional profiling and personalized PageRank analysis to predict regulatory transcription factors, and a pooled *in vivo* RNA interference (RNAi) loss-of-function screen targeting putative T_{RM} cell

[1]Division of Biological Sciences, University of California, San Diego, La Jolla, California, USA. [2]Bioinformatics and Systems Biology Graduate Program, University of California, San Diego, La Jolla, California, USA. [3]Department of Immunology and Microbiology, The Scripps Research Institute, Jupiter, Florida, USA. [4]Division of Vaccine Discovery, La Jolla Institute for Allergy and Immunology, La Jolla, California, USA. [5]Division of Infectious Diseases, Department of Medicine, University of California, San Diego, La Jolla, California, USA. [6]Department of Chemistry and Biochemistry, University of California, San Diego, La Jolla, California, USA. [7]Department of Cellular and Molecular Medicine, University of California, San Diego, La Jolla, California, USA.
*These authors contributed equally to this work.

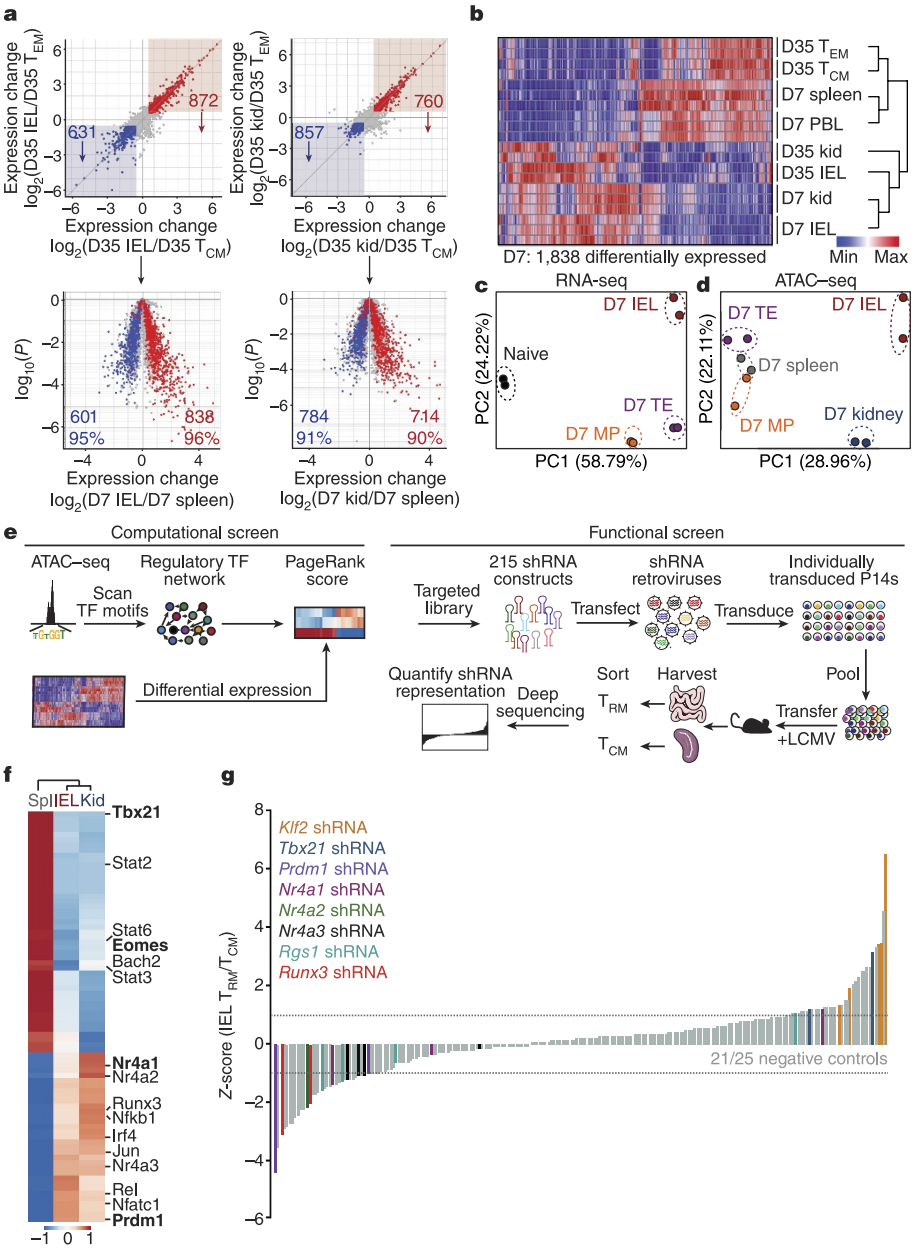

Figure 1 | Computational and loss-of-function RNAi screens identify transcriptional regulators of T_{RM} cell differentiation. a, Top, comparison of gene expression of IELs (left) and kidney T_{RM} cells (right) relative to T_{CM} and T_{EM} subsets on day 35 of LCMV infection. Red denotes genes increased in T_{RM} relative to T_{CM} and T_{EM} cells; blue denotes genes increased in T_{CM} and T_{EM} relative to T_{RM} cells. Bottom, comparison of differentially expressed genes in mature T_{RM} cells (from top panel) in cells from the spleen, IELs or kidney on day 7 of infection. **b**, Differentially expressed genes between splenic, IEL and kidney populations on day 7 of infection were compared among effector and memory $CD8^+$ T cell subsets. Populations are ordered by hierarchical clustering with Pearson correlation. **c**, PCA of differentially expressed genes among day 7 subsets and naive P14 cells. MP, memory precursors; TE, terminal effectors. **d**, PCA of differential global chromatin accessibility of subsets on day 7 of infection identified by ATAC–seq analysis. **e**, Combinatorial screening approach. TF, transcription factors. **f**, Transcription factors with a PageRank score of $\geq$1.5-fold change for day 7 non-lymphoid cells compared to day 7 splenic cells are included in the heat map; proteins known to regulate T_{RM} cell formation are in bold font. **g**, Enrichment of shRNAmir constructs in IEL T_{RM} cells relative to splenic T_{CM} cells from the RNAi screen, reported as the average *Z*-score from 3 independent screens, in which each independent screen was performed by pooling DNA from sorted P14 cells from $n = 15$, $n = 18$ and $n = 18$ mice. Each time point represents an individual experiment consisting of 2–3 biological replicates, in which cells from 2–10 mice were pooled for each replicate (**a**–**d**).

regulators identified through the computational approach (Fig. 1e). We recently demonstrated that analysis of accessible transcription factor-binding motifs and target gene expression yielded insight into factors with regulatory functions in the differentiation of circulating memory $CD8^+$ T cells[14]. Using this approach and the personalized PageRank analysis[15], we predicted several transcription factors with established regulatory roles in controlling T_{RM} cell differentiation (such as Blimp1[6], Nr4a1[11], Eomes[12] and T-bet[12,13]) and many with no previously described role in T_{RM} cells (Fig. 1f, Supplementary Table 1). We evaluated both barrier (IEL) and non-barrier (kidney) T_{RM} cells to reveal transcription factors important to T_{RM} cell differentiation independent of the tissue. In addition, a key strength of this computational screen is that influential roles of differentially expressed transcription factors as well as those with homogenous expression can be anticipated (Extended Data Fig. 2b). To establish functional relevance for predicted regulators of T_{RM} cell formation identified

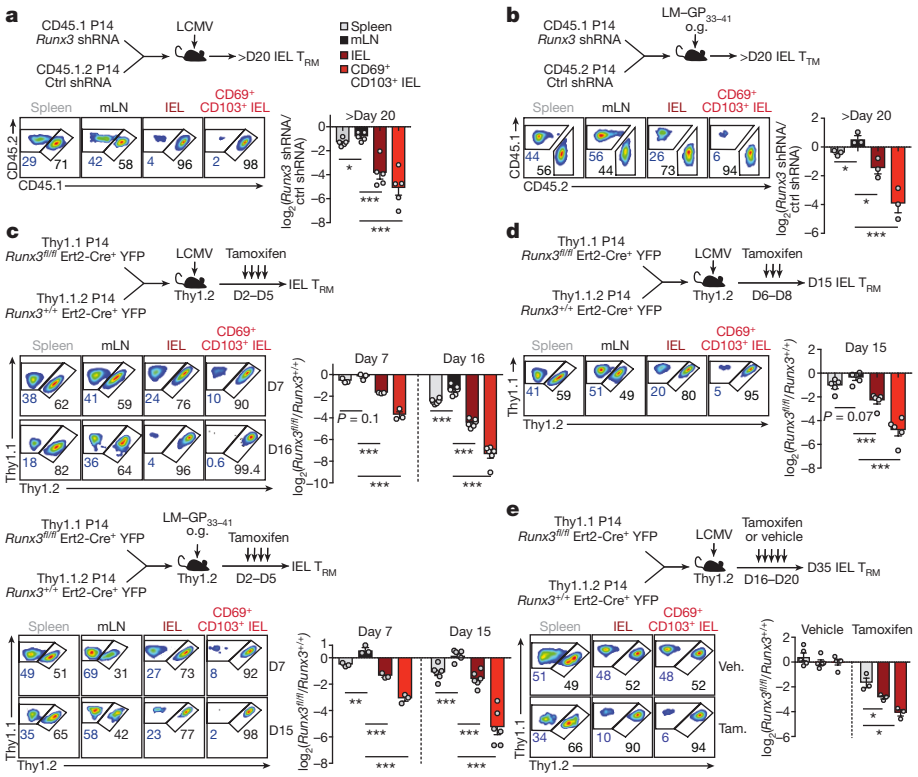

Figure 2 | Runx3 is essential for the differentiation and long-term maintenance of CD8$^+$ T_{RM} cells. a, Congenically distinct P14 cells were transduced with retroviruses encoding *Runx3* shRNAmir or a control (ctrl) shRNAmir, mixed at a 1:1 ratio, and transferred to recipient mice subsequently infected with LCMV, and the ratio of transduced cells was evaluated on day 23 or 26 in the indicated tissues. mLN, mesenteric lymph nodes. **b**, Ratio of transduced transferred cells in indicated tissues on day 32 of enteric LM–$GP_{33–41}$ infection. o.g., oral gavage. **c**, Ratio of transferred *Runx3*$^{fl/fl}$ Ert2-Cre$^+$ YFP (*Runx3*$^{fl/fl}$) to *Runx3*$^{+/+}$ Ert2-Cre$^+$ YFP (*Runx3*$^{+/+}$) P14 cells in indicated tissues on days 6/7 and 15/16 of LCMV infection (top) or enteric LM–$GP_{33–41}$ infection (bottom). **d**, Ratio of *Runx3*$^{fl/fl}$ to *Runx3*$^{+/+}$ P14 cells on day 15 of LCMV infection. **e**, Ratio of *Runx3*$^{fl/fl}$ to *Runx3*$^{+/+}$ P14 cells on day 35 of infection. Data are mean ± s.e.m of $n = 5$ (**a**), $n = 3$ (**b**), $n = 3$ (day 7) and $n = 6$ (day 15/16) (**c**), $n = 5$ (**d**), and $n = 5$ (vehicle) and $n = 3$ (tamoxifen) (**e**). All data are from one representative experiment of 2 independent experiments, except in **a**, which is pooled from 2 independent experiments. $*P < 0.05$, $**P < 0.01$, $***P < 0.005$ (Student's *t*-test). Symbols represent an individual mouse (**a**–**e**).

through PageRank analysis, we used an RNAi screening strategy[16] to test hundreds of individual microRNA-based short hairpin RNA (shRNAmir) constructs in parallel for the ability to promote or repress T_{RM} cell differentiation *in vivo* (Fig. 1g, Supplementary Table 2). Several transcription factors with established roles in regulating T_{RM} cells were identified (such as Nr4a1[13], Blimp1[6], Klf2[17] and T-bet[12,13]), as well as factors with previously unknown functions in controlling CD8$^+$ T_{RM} formation such as Nr4a3 and Runx3 (Fig. 1g).

Runx3 is a well-established regulator of CD8$^+$ T cell thymocyte development[18], supports cytotoxic activity of mature CD8$^+$ T cells[19,20], and controls CD4$^+$ T cell localization within the intestinal epithelium[21]. Although little is known regarding a role for Runx3 in CD8$^+$ T_{RM} cells, both computational and functional screens identified Runx3 as a putative regulator of T_{RM} cell fate specification (Fig. 1f, g) despite relatively uniform *Runx3* expression in circulating and resident CD8$^+$ T cell subsets (Extended Data Figs 2b, 3a). We validated a role for Runx3 through a 1:1 mixed transfer of P14 cells transduced with control (*Cd19* shRNAmir) or *Runx3* shRNAmir-encoding retroviruses into mice that were subsequently infected with LCMV (Fig. 2a). *Runx3* shRNAmir suppressed *Runx3* expression (Extended Data Fig. 3b) and impaired the formation of IEL T_{RM} cells relative to circulating cells (Fig. 2a and Extended Data Fig. 3c, d), consistent with the RNAi screen. Furthermore, *Runx3* RNAi also impaired T_{RM} cell differentiation in the context of a localized enteric infection with *Listeria monocytogenes* expressing $GP_{33–41}$ (LM–$GP_{33–41}$) (Fig. 2b).

Next, using a tamoxifen-inducible deletion approach, *Runx3*$^{fl/fl}$ Ert2-Cre$^+$ P14 (*Runx3*$^{fl/fl}$) or *Runx3*$^{+/+}$ Ert2-Cre$^+$ P14 (*Runx3*$^{+/+}$) cells were mixed 1:1 and transferred into host mice followed by LCMV or enteric LM–$GP_{33–41}$ infection (Fig. 2c). *Runx3*-deficiency resulted in a 2–6-fold loss of splenocytes and minimal loss of mesenteric lymph node cells by day 15/16 of infection. However, *Runx3*-deficiency resulted in a 50–150-fold loss of CD69$^+$CD103$^+$ T_{RM} cells in both infection settings (Fig. 2c and Extended Data Fig. 3e). Moreover, delaying tamoxifen treatment to days 6–8 or 16–20 of infection further emphasized a distinct dependence of T_{RM} cell differentiation on Runx3 (Fig. 2d) as well as a crucial role for Runx3 in maintaining T_{RM} cell homeostasis (Fig. 2e, Extended Data Fig. 3f). Furthermore, Runx3 was necessary for optimal T_{RM} cell differentiation of H-2D^b $GP_{33–41}$ tetramer$^+$ cells (Extended Data Fig. 4a–d). Taken together, these data demonstrate that Runx3 is crucial for T_{RM} cell differentiation and maintenance.

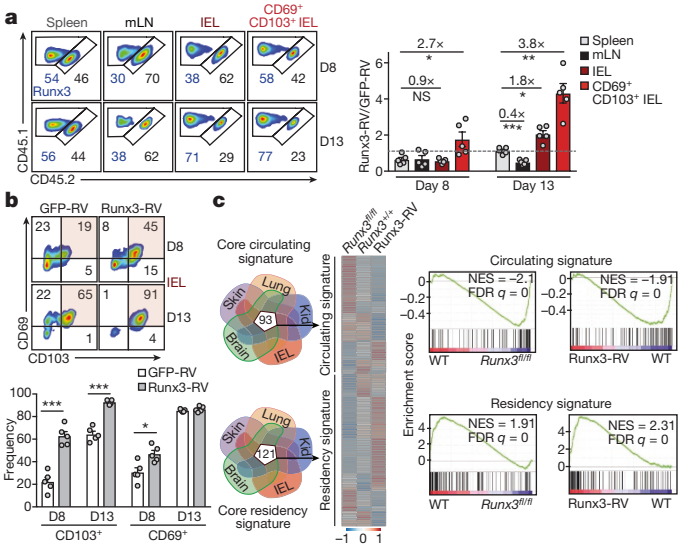

Figure 3 | Runx3 programs CD8$^+$ T cell tissue-residency. a, Congenically distinct P14 cells were transduced with retroviruses encoding Runx3-cDNA (Runx3-RV; CD45.1$^+$ cells) or control GFP (GFP-RV; CD45.1.2$^+$ cells), mixed at a 1:1 ratio, and transferred to recipient mice subsequently infected with LCMV. Ratios of transduced cells were evaluated on days 8 and 12/13 of infection. **b**, Frequency of CD69$^+$ and CD103$^+$ cells from **a**. **c**, Left, relative expression of the core 'circulating' and 'residency' genes between Runx3-RV, *Runx3*$^{fl/fl}$ and *Runx3*$^{+/+}$ CD8$^+$ T cells. Right, gene set enrichment analysis (GSEA). FDR, false discovery rate; NES, normalized enrichment score; WT, wild type. Data are mean ± s.e.m of $n = 5$ mice (**a**, **b**) from one representative experiment of 2 independent experiments. $*P < 0.05$, $**P < 0.01$, $***P < 0.005$ (Student's *t*-test). NS, not significant. Symbols represent an individual mouse (**a**, **b**).

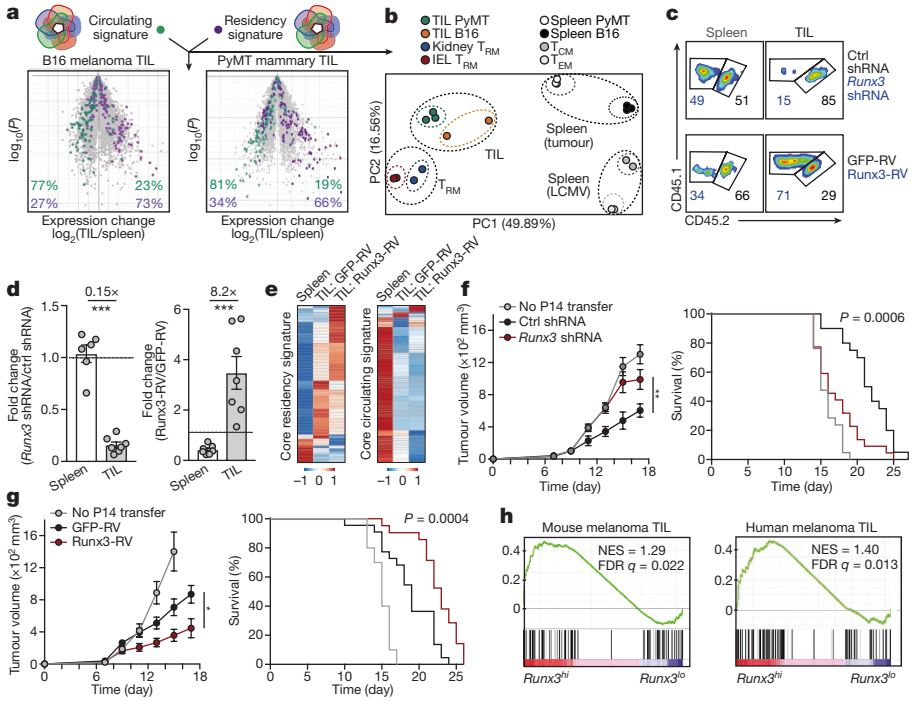

Figure 4 | CD8$^+$ TILs share transcriptional signatures with T_{RM} cells and require Runx3 for tumour residency. a, Comparison of the core tissue-residency signature and core circulating signature (from Fig. 3c) in B16 melanoma CD8$^+$ TILs[27] or PyMT mammary tumour CD8$^+$ TILs[27] relative to corresponding splenic cells. **b**, PCA of gene expression of the core tissue-residency and circulating gene sets for TILs, T_{RM} cells or splenic subsets. **c**, **d**, Congenically distinct P14 cells were transduced with retroviruses encoding *Runx3* shRNAmir or Runx3-RV (CD45.1$^+$ cells) and control shRNAmir or GFP-RV (CD45.1.2$^+$ cells), mixed at a 1:1 ratio and transferred into mice with established B16-GP$_{33–41}$ melanoma tumours. Flow plots and graphs indicate ratio of transduced cells. **e**, Relative expression of the core tissue-residency and core circulating gene sets in GFP-RV splenocytes, GFP-RV TILs, and Runx3-RV TILs following the same approach as in **c**. **f**, **g**, Tumour growth and survival after adoptive transfer of the indicated cell population. A log-rank (Mantel–Cox) test was used to compare survival rates. **h**, GSEA of the core tissue-residency signature in *Runx3*^{hi} versus *Runx3*^{lo} TIL from single-cell RNA-seq analyses of mouse[29] and human[30] melanoma TILs. Data are mean ± s.e.m of $n = 5$ (*Runx3* shRNAmir) or $n = 7$ mice per group (Runx3-RV) from one representative experiment of 3 independent experiments (**c**, **d**) or data pooled from 3 independent experiments consisting of $n = 21$ (no P14), $n = 20$ (control shRNAmir), $n = 22$ (*Runx3* shRNAmir) (**f**), $n = 10$ (no P14), $n = 22$ (GFP-RV), $n = 21$ (Runx3-RV) mice per group (**g**). $^*P < 0.05$, $^{**}P < 0.01$, $^{***}P < 0.005$ (Student's *t*-test). Symbols represent an individual mouse (**d**).

Runx3 deletion also resulted in a loss of T_{RM} cells in non-barrier tissues (salivary gland and kidney; Extended Data Fig. 5a, b), and optimal T_{RM} cell differentiation in the skin and lung parenchyma required Runx3 (Extended Data Fig. 5c–h). Thus, the loss of T_{RM} cells in a range of non-lymphoid tissues indicated that Runx3 drives the formation of T_{RM} cells independently of the tissue site. Furthermore, Runx3 was required for maximal expression of granzyme B in T_{RM} cells, although cytokine production was unchanged (Extended Data Fig. 6a, b). *Runx3*-deficiency resulted in a greater frequency of annexin V$^+$ cells (Extended Data Fig. 6c, d), most prominently in the CD69$^+$CD103$^+$ T_{RM} population; thus, the marked loss of T_{RM} cells was at least in part due to a greater rate of apoptosis, as proliferation and trafficking were not affected (Extended Data Fig. 6e, f).

We next assessed whether enhanced expression of Runx3 could augment T_{RM} cell differentiation. Overexpression of Runx3 accelerated IEL P14 CD69$^+$CD103$^+$ T_{RM} cell differentiation on day 8 of infection, but did not affect migration to the small intestine (Fig. 3a). Evidence of enhanced T_{RM} cell differentiation was further confirmed by the greater abundance of IEL T_{RM} cells on day 12/13 of infection and enhanced CD103 expression, consistent with a reported role for Runx3 in regulating CD103 expression[21,22] (Fig. 3b). Furthermore, overexpression of Runx3 also boosted T_{RM} cell differentiation in the lung parenchyma (Extended Data Fig. 7a–d).

Given that manipulation of Runx3 affected T_{RM} cell formation in diverse tissue microenvironments, we constructed a core T_{RM} cell transcriptional signature by computational integration of CD8$^+$ T_{RM} gene-expression datasets from small intestine IELs, kidney, lung[5], skin[5] and brain[7], to evaluate the hypothesis that Runx3 is a universal regulator of T_{RM} cell specification (Fig. 3c, Supplementary Table 3). Notably, we found that most of the core tissue-residency signature genes were upregulated in Runx3-overexpressing cells and downregulated in *Runx3*-deficient cells. Conversely, the core signature of circulating memory cells was enriched in *Runx3*-deficient cells and depleted from Runx3-overexpressing cells (Fig. 3c). Therefore, Runx3 promoted the expression of tissue-residency signature genes and repressed genes characteristic of circulating cells. This conclusion was further corroborated by chromatin-immunoprecipitation followed by deep sequencing (ChIP–seq) analysis[23], indicating that Runx3 binding was enriched in both core tissue-residency and circulating genes relative to background sites (Extended Data Fig. 8a).

Through evaluation of accessible Runx3-binding motifs from ATAC–seq analysis, we generated a regulatory Runx3-binding network (Extended Data Fig. 8b) and found that Runx3 putatively regulates a distinct network of genes in differentiating IEL-T_{RM} precursor cells relative to splenic effector cells, including selective enrichment of genes linked to cell adhesion and regulation of transcription factor activity. In connection, Runx3 has been shown to cooperate with the transcription factor T-bet in many contexts[19,24], yet T-bet is a potent suppressor of early T_{RM} cell differentiation[12,13]. ChIP–seq data[23] indicated that Runx3 directly binds to multiple sites of the *Tbx21* locus (encoding T-bet; Extended Data Fig. 8c), and *Runx3*-deficient CD8$^+$ T cells exhibited increased T-bet levels (Extended Data Fig. 8d). *Tbx21* RNAi in *Runx3*-deficient cells enhanced T_{RM} cell numbers in the IEL compartment and restored CD103 and CD69 expression (Extended Data Fig. 8e, f), but did not fully rescue T_{RM} cell differentiation. These findings are consistent with Runx3 regulating multiple targets that

influence T_{RM} cell formation (Fig. 3c), including suppression of canonical genes associated with tissue egress (Extended Data Fig. 8g, h).

It has been noted that $CD8^+$ tumour-infiltrating lymphocytes (TILs) can exhibit characteristics of T_{RM} cells, and a positive prognosis has been correlated with TILs that present qualities of T_{RM} cells[25,26]. As Runx3 regulates core features of tissue residency (Fig. 3c), we assessed the transcriptional similarities of TILs and T_{RM} cells and evaluated a role for Runx3 in controlling TIL accumulation. TILs isolated from mouse melanoma[27] or mammary tumours[27] shared approximately 70% of the core tissue-residency gene-expression program relative to splenic $CD8^+$ T cells (Fig. 4a), and this relationship was further highlighted through PCA (Fig. 4b). Utilizing an adoptive therapy model, *Runx3*-RNAi or Runx3-overexpressing P14 cells were mixed with control P14 cells at a 1:1 ratio and transferred into mice with established melanoma tumours expressing $GP_{33–41}$ (Extended Data Fig. 9a). *Runx3*-deficiency impaired TIL accumulation (Fig. 4c, d) without affecting migration to the tumour (Extended Data Fig. 9b). Alternatively, Runx3-overexpression enhanced TIL abundance (Fig. 4c, d), expression of granzyme B (Extended Data Fig. 9c) and certain core tissue-residency genes while further suppressing core circulating genes (Fig. 4e). In clinical settings, TIL density strongly correlates with positive outcomes[28], and we observed *Runx3*-deficient P14 cells were impaired in their ability to control tumour growth, resulting in greater mortality (Fig. 4f). Conversely, Runx3-overexpressing cells delayed tumour growth and prolonged survival (Fig. 4g). Notably, human $CD8^+$ TILs also exhibited enrichment of the core tissue-residency signature relative to circulating $CD8^+$ T cells[25] (Extended Data Fig. 9d), and analysis of single-cell RNA sequencing (RNA-seq) data from mouse[29] and human melanoma TILs[30] indicated that activated $CD44^+CD8^+$ T cells expressing *Runx3* exhibited enrichment of the tissue-residency gene-expression signature relative to $CD44^+CD8^+$ TILs with low *Runx3* expression levels (Fig. 4h). These data indicate that in both human and mouse TILs, tissue-residency features are driven by Runx3. In connection, it was recently demonstrated that human lung cancer TILs enriched with certain qualities of T_{RM} cells also correlated with TIL abundance and a positive prognosis[26]. Thus, the manipulation of transcription factors that promote tissue residency may yield more effective TILs and anti-viral memory T cells by supplementing $CD8^+$ T cells with a gene-expression program that better supports features important to both T_{RM} cells and TILs such as *in situ* survival, tissue retention, and repression of egress, ultimately fostering accumulation of protective T cells in tissues.

Online Content Methods, along with any additional Extended Data display items and Source Data, are available in the online version of the paper; references unique to these sections appear only in the online paper.

Received 26 May; accepted 31 October 2017.
Published online 6 December 2017.

1. Jiang, X. *et al.* Skin infection generates non-migratory memory $CD8^+$ T_{RM} cells providing global skin immunity. *Nature* **483,** 227–231 (2012).
2. Schenkel, J. M. *et al.* T cell memory. Resident memory CD8 T cells trigger protective innate and adaptive immune responses. *Science* **346,** 98–101 (2014).
3. Chang, J. T., Wherry, E. J. & Goldrath, A. W. Molecular regulation of effector and memory T cell differentiation. *Nat. Immunol.* **15,** 1104–1115 (2014).
4. Mueller, S. N., Gebhardt, T., Carbone, F. R. & Heath, W. R. Memory T cell subsets, migration patterns, and tissue residence. *Annu. Rev. Immunol.* **31,** 137–161 (2013).
5. Mackay, L. K. *et al.* The developmental pathway for $CD103^+CD8^+$ tissue-resident memory T cells of skin. *Nat. Immunol.* **14,** 1294–1301 (2013).
6. Mackay, L. K. *et al.* Hobit and Blimp1 instruct a universal transcriptional program of tissue residency in lymphocytes. *Science* **352,** 459–463 (2016).
7. Wakim, L. M. *et al.* The molecular signature of tissue resident memory CD8 T cells isolated from the brain. *J. Immunol.* **189,** 3462–3471 (2012).
8. Masopust, D., Vezys, V., Wherry, E. J., Barber, D. L. & Ahmed, R. Cutting edge: gut microenvironment promotes differentiation of a unique memory CD8 T cell population. *J. Immunol.* **176,** 2079–2083 (2006).
9. Sheridan, B. S. *et al.* Oral infection drives a distinct population of intestinal resident memory $CD8^+$ T cells with enhanced protective function. *Immunity* **40,** 747–757 (2014).
10. Masopust, D. *et al.* Dynamic T cell migration program provides resident memory within intestinal epithelium. *J. Exp. Med.* **207,** 553–564 (2010).
11. Boddupalli, C. S. *et al.* ABC transporters and NR4A1 identify a quiescent subset of tissue-resident memory T cells. *J. Clin. Invest.* **126,** 3905–3916 (2016).
12. Mackay, L. K. *et al.* T-box transcription factors combine with the cytokines TGF-β and IL-15 to control tissue-resident memory T cell fate. *Immunity* **43,** 1101–1111 (2015).
13. Laidlaw, B. J. *et al.* $CD4^+$ T cell help guides formation of $CD103^+$ lung-resident memory $CD8^+$ T cells during influenza viral infection. *Immunity* **41,** 633–645 (2014).
14. Yu, B. *et al.* Epigenetic landscapes reveal transcription factors that regulate $CD8^+$ T cell differentiation. *Nat. Immunol.* **18,** 573–582 (2017).
15. Page, L., Brin, S., Motwani, R. & Winograd, T. The PageRank citation ranking: Bringing order to the web. *Technical Report, Stanford InfoLab* (1998).
16. Chen, R. *et al. In vivo* RNA interference screens identify regulators of antiviral $CD4^+$ and $CD8^+$ T cell differentiation. *Immunity* **41,** 325–338 (2014).
17. Skon, C. N. *et al.* Transcriptional downregulation of *S1pr1* is required for the establishment of resident memory $CD8^+$ T cells. *Nat. Immunol.* **14,** 1285–1293 (2013).
18. Taniuchi, I. *et al.* Differential requirements for Runx proteins in CD4 repression and epigenetic silencing during T lymphocyte development. *Cell* **111,** 621–633 (2002).
19. Cruz-Guilloty, F. *et al.* Runx3 and T-box proteins cooperate to establish the transcriptional program of effector CTLs. *J. Exp. Med.* **206,** 51–59 (2009).
20. Shan, Q. *et al.* The transcription factor Runx3 guards cytotoxic $CD8^+$ effector T cells against deviation towards follicular helper T cell lineage. *Nat. Immunol.* **18,** 931–939 (2017).
21. Reis, B. S., Rogoz, A., Costa-Pinto, F. A., Taniuchi, I. & Mucida, D. Mutual expression of the transcription factors Runx3 and ThPOK regulates intestinal $CD4^+$ T cell immunity. *Nat. Immunol.* **14,** 271–280 (2013).
22. Grueter, B. *et al.* Runx3 regulates integrin α E/CD103 and CD4 expression during development of $CD4^-/CD8^+$ T cells. *J. Immunol.* **175,** 1694–1705 (2005).
23. Lotem, J. *et al.* Runx3-mediated transcriptional program in cytotoxic lymphocytes. *PLoS One* **8,** e80467 (2013).
24. Reis, B. S., Hoytema van Konijnenburg, D. P., Grivennikov, S. I. & Mucida, D. Transcription factor T-bet regulates intraepithelial lymphocyte functional maturation. *Immunity* **41,** 244–256 (2014).
25. Djenidi, F. *et al.* $CD8^+CD103^+$ tumor-infiltrating lymphocytes are tumor-specific tissue-resident memory T cells and a prognostic factor for survival in lung cancer patients. *J. Immunol.* **194,** 3475–3486 (2015).
26. Ganesan, A.-P. *et al.* Tissue-resident memory features are linked to the magnitude of cytotoxic T cell responses in human lung cancer. *Nat. Immunol.* **18,** 940–950 (2017).
27. Doedens, A. L. *et al.* Molecular programming of tumor-infiltrating $CD8^+$ T cells and IL15 resistance. *Cancer Immunol. Res.* **4,** 799–811 (2016).
28. Gooden, M. J., de Bock, G. H., Leffers, N., Daemen, T. & Nijman, H. W. The prognostic influence of tumour-infiltrating lymphocytes in cancer: a systematic review with meta-analysis. *Br. J. Cancer* **105,** 93–103 (2011).
29. Singer, M. *et al.* A distinct gene module for dysfunction uncoupled from activation in tumor-infiltrating T cells. *Cell* **166,** 1500–1511.e9 (2016).
30. Tirosh, I. *et al.* Dissecting the multicellular ecosystem of metastatic melanoma by single-cell RNA-seq. *Science* **352,** 189–196 (2016).

Supplementary Information is available in the online version of the paper.

Acknowledgements We thank all the members of the Goldrath and Pipkin laboratories for their contributions. We also thank the Flow Cytometry Core at the La Jolla Institute for Allergy and Immunology. This study was funded in part by the UCSD Molecular Biology Cancer Fellowship (J.J.M.), the US National Institutes of Health U19AI109976 (S.C., M.E.P., A.W.G) and R01 AI095634 (M.E.P.), California Institute for Regenerative Medicine RB5-07012 (W.W.), the Kimmelman Family Foundation and the San Diego Center for Precision Immunotherapy (A.W.G.).

Author Contributions J.J.M. designed and performed experiments, analysed the data and wrote the manuscript; C.T. assisted with the RNAi screen, transfections, transductions, tissue processing, and tumour models; B.Y. performed the computational analyses and ATAC–seq experiment; K.Z. assisted with computational analyses; K.O. and T.N. assisted with tissue processing, analysis, and qPCR; A.T.P assisted with tissue processing, inducible deletion experiments, and analysis; D.W. and A.J.G. helped with the inducible deletion experiments, RNA-seq analysis, and tumour models; S.C. provided reagents and advice; W.W. supervised the computational analysis and contributed advice; M.E.P. and A.W.G. supervised the project, designed experiments, and wrote the manuscript.

Author Information Reprints and permissions information is available at www.nature.com/reprints. The authors declare no competing financial interests. Readers are welcome to comment on the online version of the paper. Publisher's note: Springer Nature remains neutral with regard to jurisdictional claims in published maps and institutional affiliations. Correspondence and requests for materials should be addressed to M.E.P. (mpipkin@scripps.edu) or A.W.G. (agoldrath@ucsd.edu).

Reviewer Information *Nature* thanks F. Carbone, D. Mucida, A. Schietinger and the other anonymous reviewer(s) for their contribution to the peer review of this work.

METHODS

Mice. Mice were maintained in specific-pathogen-free conditions in accordance with the Institutional Animal Care and Use Committees (IACUC) of the University of California, San Diego (UCSD) and The Scripps Research Institute, Jupiter, Florida (TSRI-FL). All mice were of a C57BL6/J background and bred at UCSD and TSRI-FL or purchased from the Jackson Laboratory, including: wild-type or P14 mice with distinct expression of the congenic molecules CD45.1, CD45.2, Thy1.1 and Thy1.2 as well as control Thy1.1^{+}Thy1.2^{+} *Runx3*$^{+/+}$ Ert2-Cre^{+} YFP P14 mice and *Runx3* inducible deletion Thy1.1^{+} *Runx3*$^{fl/fl}$ Ert2-Cre^{+} YFP P14 mice. *Runx3*$^{+/+}$dLck-Cre^{+} YFP and *Runx3*$^{fl/fl}$ dLck-Cre^{+} YFP mice were used for studying polyclonal CD8^{+} T cell responses. Male and female mice were used for experiments, and were age and sex matched, between 1.5 and 4 months old, and randomly assigned to experimental groups. The *Rosa26* stop-flox enhanced yellow fluorescent protein (eYFP) reporter mice were used for all *Runx3*-deletion experiments. Cre-mediated deletion disrupts the *Runx3* DNA-binding domain in exon 4, which exists in transcripts originating from both the distal and proximal promoter. Thus, both long and short *Runx3* forms are inactivated in these alleles.

Naive T cell transfers, infection and treatments. Naive P14 CD8^{+} T cells were transferred intravenously into congenically distinct sex-matched recipient mice, or female P14 cells were transferred into male mice. For all microarray, RNA-seq or ATAC–seq experiments, a total of 1×10^5 P14 cells were transferred. For co-transfer experiments, naive Thy1.1^{+}Thy1.2^{+} *Runx3*$^{+/+}$ Ert2-Cre YFP^{+} P14 cells and naive Thy1.1^{+} *Runx3*$^{fl/fl}$ Ert2-Cre YFP^{+} P14 cells were mixed 1:1 and a total of 3×10^4 P14 cells were transferred into Thy1.2^{+} recipient mice. Recipient mice were subsequently infected intraperitoneally with 2×10^5 plaque-forming units (PFU) of the Armstrong strain of LCMV or 10^{10} colony-forming units (CFU) of *L. monocytogenes* expressing $GP_{33–41}$ via oral gavage[9] one day after cell transfer. For induced *Runx3* deletion, recipient mice were intraperitoneally treated with 1 mg of tamoxifen diluted in sunflower oil on days 0–4, 2–5 or 6–8 of infection. For late deletion of *Runx3* (days 16–20), recipient mice were treated with 2 mg of tamoxifen via oral gavage.

For T_{RM} precursor experiments, 1×10^5 P14 cells were transferred, recipient mice were infected with LCMV the next day, and KLRG1^{lo} or KLRG1^{hi} P14 cells from spleens and lymph nodes were sorted on day 5 of infection. Sorted cells (1×10^5) were transferred into recipient mice infected 4 days previously with LCMV. The number of CD62L^{+} T_{CM}, CD62L^{-} T_{EM}, or IEL T_{RM} cells were evaluated on days 20–25 of infection using flow cytometry.

To distinguish vascular-associated CD8^{+} T cells in non-lymphoid tissues, 3 μg of CD8α (53-6.7) conjugated to allophycocyanin (APC) eFlour780 was injected intravenously into mice four minutes before euthanization and organ excision. CD8α^{neg} cells were considered to be localized within non-lymphoid tissues.

Preparation of cell suspensions. Isolation of CD8^{+} T cells was performed similarly as described[31]. For isolation of CD8^{+} T cells from the small intestine IEL compartment, Peyer's patches were removed and the intestine was cut longitudinally and subsequently cut laterally into 0.5–1 cm^2 pieces that were then incubated with 0.154 mg ml^{-1} dithioerythritol (DTE) in 10% HBSS/HEPES bicarbonate for 30 min at 37 °C while stirring. Kidneys, salivary glands, and lungs were cut into pieces and digested for 30 min with 100 U ml^{-1} type I collagenase (Worthington) in RPMI 1640, 5% FBS, 2 mM $MgCl_2$, 2 mM $CaCl_2$ at 37 °C while shaking. Skin was processed similarly as previously described[32], in which a 2 cm^2 area of the right flank was excised, pre-digested for 30 min at 37 °C and then enzymatically digested with 0.7 mg ml^{-1} collagenase D. After enzymatic incubations (skin, lungs, kidneys and salivary glands), tissues were further dissociated over a 70-μm nylon cell strainer (Falcon). For isolation of lymphocytes, single-cell suspensions were then separated using a 44/67% Percoll density gradient. Spleens and lymph nodes were processed with the frosted ends of microscope slides. Red blood cells were lysed with ACK buffer (140 mM NH_4Cl and 17 mM Tris-base, pH 7.4).

Antibodies, intracellular staining, flow cytometry and cell sorting. The following antibodies were obtained from eBioscience: CD8α (53-6.7), CD8β (eBio H35-17.2), CD62L (MEL-14), CD127 (A7R34), KLRG1 (2F1), CD103 (2E7), CD69 (H1.2F3), CD45.1 (A20-1.7), CD45.2 (104), Thy1.1 (OX-7, HIS51), Thy1.2 (53-2.1), CCR9 (Ebio CW-1.2), CXCR3 (CXCR3-173), CD49d (R1-2), TNF (MP6-XT22), GzB (GB11), PD-1 (J43), Tim3 (RMT3-23), Lag3 (eBioC9B7N), KI-67 (SolA15), and IFNγ (XMG1.2) or from BioLegend: CD62L (MEL-14), CD103 (2E7), CD69 (H1.2F3), CD45.1 (A20-1.7), Thy1.1 (OX-7), Thy1.2 (30-H12), and T-bet (4B10). For analysis of apoptosis, the Annexin V Apoptosis Detection Kit was used per manufacturer instructions (eBioscience); propidium-iodide-negative cells were analysed for annexin V staining. The H-2D^{b} $GP_{33–41}$ tetramer was obtained from the NIH Tetramer Core. For intracellular staining of cytokines or transcription factors while preserving ametrine or YFP reporter expression in transduced or Cre-YFP^{+} populations, cells were fixed and permeabilized through a 10 min incubation with BD cytofix/cytoperm (BD Biosciences). Intracellular staining was subsequently performed using the Permeabilization Buffer of the Foxp3-Transcription Factor Staining Buffer Set (eBioscience). To assess cytokine production, CD8^{+} T cells were re-stimulated with the $GP_{33–41}$ peptide in the presence of Protein Transport Inhibitor Cocktail (eBioscience). For flow cytometry analysis, all events were acquired on a BD LSRFortessa X-20 or a BD LSRFortessa. Cell sorting was performed on BD FACSAria or BD FACSAria Fusion instruments.

RNAi screening approach. We have described this screening approach in detail previously[16]. The targeted shRNAmir library was generated on the basis of key genes identified from the computational screening approach as well as genes with known roles in regulating T_{RM} cells from literature. The library was produced by cloning shERWOOD-designed shRNAmir sequences[33], after PCR of synthetic 97-mer oligonucleotides, into our pLMPd-Amt vector[16]. Purified DNA from sequence-verified clones was used to package retroviral particles in PLAT-E cells. The PLAT-E cell line was obtained from Cell Biolabs and were not authenticated or tested for mycoplasma contamination before use. For transfections, PLAT-E cells were seeded in the middle 60 wells of a 96-well flat-bottom plate at a density of 4×10^4–6×10^4 cells per well one day before transfection. Next, each well was individually transfected with 0.2 μg of DNA from each pLMPd-Amt clone and 0.2 μg of pCL-Eco using TransIT-LT1 (Mirus). Retroviral supernatant was collected 36, 48 and 60 h after transfection, and retroviral supernatant from each well was used to individually transduce *in vitro* activated P14 cells in 96-well round-bottom plates.

For CD8^{+} T cell activation *in vitro*, naive CD8^{+} T cells from spleen and lymph nodes were negatively enriched and 2×10^5 P14 cells were plated in the middle 60 wells of 96-well round-bottom plates pre-coated with 100 μg ml^{-1} goat anti-hamster IgG (H+L, Thermo Fisher Scientific) and 1 μg ml^{-1} anti-CD3 (145-2C11) and 1 μg ml^{-1} anti-CD28 (37.51) (both from eBioscience). Culture medium was removed 18 h after activation, and replaced with retroviral supernatant supplemented with 50 μM BME and 8 μg ml^{-1} polybrene (Millipore) followed by spinfection (60 min centrifugation at 805*g*, 37 °C). Two hours after the spinfection, the P14 cells were washed three times with cold PBS and 90% of each well of cells (individually transduced with distinct retroviral constructs) was collected, pooled and 5×10^5 pooled P14 cells were transferred into recipient mice, which were then infected 1 h later with 1.5×10^5 PFU of LCMV clone 13 intraperitoneally, resulting in an acute infection[16]. The remaining cells *in vitro* were cultured for an additional 24 h and either pooled for 'input' sequencing (6×10^5 P14 cells) or were used to test transduction efficiency of each construct using flow cytometry to detect the percentage of ametrine^{+} cells in each well.

Twelve days after infection, spleens and small intestines were collected from 15–18 mice and splenocytes and IEL P14 cells were processed as described above. Before sorting, all IEL or splenic samples were pooled. CD62L^{+} P14 cells (T_{CM}) from the spleen as well as P14 cells from the IEL were sorted (2×10^5–6×10^5 cells total). Genomic DNA was then collected from sorted cells using the FlexiGene kit (Qiagen). The integrated proviral passenger strand shRNAmir sequences in each cell subset were amplified from 20–100 ng total genomic DNA per reaction, with 23–28 cycles of PCR using Ion Proton-compatible barcoded primers that anneal to the common 5′ mir30 and shRNAmir loop sequences. Between two and three replicate reactions were performed for each genomic DNA sample and the replicates were pooled after amplification. The pooled reactions were purified using AMPure XP beads, the amplicons in each sample were quantified using a Bioanalyzer, and then pooled in a 1:1 molar ratio for sequencing. In each replicate of the screen, a minimum of 2.5 million reads per sample were generated and retained, after filtering low-quality reads. Reads assigned to each barcode were aligned to a reference database of all shRNAmirs in the library using BLAST and a custom script to count the top alignment of each read and summarize the number of reads aligned to each shRNAmir.

For analysis of shRNAmir representation in T_{CM} cells relative to IEL T_{RM}, the total number of reads in each of the samples was normalized, and the number of reads for each shRNAmir was scaled proportionally. Subsequently, the normalized number of reads in the IEL T_{RM} cells for a given shRNAmir was divided by the normalized number of reads for the same shRNAmir in the T_{CM} sample and then $\log_2$ transformed. The mean and s.d. of the ratios of each of the 25 negative-control shRNAmir constructs (targeting *Cd19*, *Cd4*, *Cd14*, *Ms4a1*, *Cd22*, *Hes1*, *Klf12*, *Mafb*, *Plagl1*, *Pou2af1* and *Smarca1*) were used to calculate the *Z*-score for each shRNAmir construct. The screen was repeated three times and the *Z*-score of each construct from each individual screen was averaged and plotted (Fig. 1g Supplementary Table 2). Certain constructs were added after the first screen or were not detectable in one of the screens, but all constructs were successfully screened 2–3 times except for 13 constructs, which are marked by an asterisk in Supplementary Table 2. Eighty-four per cent (21 out of 25) of all negative control shRNAmir constructs had an average *Z*-score between −0.9 and 0.9.

CD8^{+} T cell transduction, cell transfer and infection for individual analysis of retroviral constructs. Activation, transfections and transductions were carried out

as described for the RNAi screening approach except in some experiments 2×10^6 P14 cells were activated per well in 6-well plates. Congenically distinct P14 cells transduced with the *Runx3.2* shRNAmir or *Cd19.1* shRNAmir (control) retroviruses were mixed 1:1 within 24 h of transduction and a total of 1×10^5–5×10^5 P14 cells were transferred intravenously into recipient mice. One hour after adoptive transfer, recipient mice were infected intraperitoneally or intratracheally with 2×10^5 PFU LCMV Armstrong or intradermally with 2×10^4 PFU clone 13. In similar experiments, P14 cells were transduced with MigR1-based retroviruses[34] that were empty (GFP-RV) or that contained *Runx3* cDNA (Runx3-RV), mixed 1:1 and transferred to recipient mice for subsequent infections. For T-bet rescue experiments, Thy1.2$^+$ *Runx3*$^{+/+}$ Ert2-Cre YFP$^+$ P14 cells were transduced with *Cd19.1* shRNAmir and Thy1.1$^+$ *Runx3*$^{fl/fl}$ Ert2-Cre YFP$^+$ P14 cells were transduced with *Tbx21.3* shRNAmir-encoding retroviruses, mixed 1:1 and transferred into recipient mice, which were infected 1 h later with LCMV Armstrong intraperitoneally and treated with 1 mg tamoxifen intraperitoneally for five consecutive days starting with the day of infection.

Adoptive therapy tumour model. For adoptive therapy experiments, 5×10^5 B16-GP$_{33}$ cells, which were treated for mycoplasma and authenticated in *in vitro* killing assays, were transplanted subcutaneously into the right flank of wild-type mice. After tumours became palpable, 7–8 days after transplantation, *in vitro* expanded P14 cells were transferred intravenously. For comparison of TIL accumulation in a mixed transfer setting, naive P14 cells were activated, transduced and expanded with 100 U ml^{-1} of IL-2 for 2–3 days; cells transduced with control constructs (*Cd19.1* shRNAmir or GFP-RV) or experimental constructs (*Runx3.2* shRNAmir or Runx3-RV) were mixed 1:1 and 0.5×10^6–1×10^6 P14 cells were transferred intravenously. For efficacy studies, transduced cells were expanded for 5–6 days; transduced cells were then sorted (or not sorted with a Runx3-RV and GFP-RV transduction efficiency >83%), and 1×10^6–2.5×10^6 cells were transferred intravenously into mice with established B16-GP$_{33}$ tumours. Tumours were monitored daily and mice with ulcerated tumours or tumours exceeding 1,500 mm^3 were euthanized, in accordance with UCSD IACUC.

Quantitative PCR, microarray, RNA-seq and ATAC–seq analysis. For validation of the Runx3-RV overexpression construct and *Runx3.2* shRNAmir construct, enriched CD8$^+$ T cells were activated, transduced, and expanded for 4–6 days in 100 U ml^{-1} IL-2. Cells were sorted on ametrine (*Runx3* shRNAmir or control shRNAmir) or GFP (Runx3-RV or GFP-RV) directly into TRIzol (Life Technologies), and RNA was extracted per manufacturer's specifications. Next, cDNA was synthesized using Superscript II (Life Technologies) and quantitative PCR (qPCR) was performed using the Stratagene Brilliant II Syber Green master mix (Agilent Technologies). *Runx3* expression levels were normalized to the housekeeping gene *Hprt*. We have previously validated the *Tbx21.3* shRNAmir[16]. The following primers were used for qPCR: *Runx3* forward, 5′-CAGGTTCAACGACCTTCGATT-3′, *Runx3* reverse, 5′-GTGGTAGGTAGCCACTTGGG-3′; *Hprt* forward, 5′-GGCCAGACTTTGTTGGATTT-3′, *Hprt* reverse, 5′-CAACTTGCGCT CATCTTAGG-3′.

On day 7 of infection, tissues from 2–3 mice were pooled and 2×10^4–3×10^4 P14 cells from the IELs, kidney, spleen or blood were sorted into TRIzol. On day 35 of infection, tissues from 5–10 mice were pooled and 1×10^4–2×10^4 CD62L$^+$ T$_{CM}$, CD62L$^-$ T$_{EM}$, kidney T$_{RM}$, and IEL T$_{RM}$ P14 cells were sorted into TRIzol. As described previously, RNA was amplified and labelled with biotin and hybridized to Affymetrix Mouse Gene ST 1.0 micrroarrays[35]. Analyses were performed using GenePattern Multiplot Studio. Differentially expressed genes in IEL T$_{RM}$ compared to T$_{CM}$ and T$_{EM}$ cells as well as kidney T$_{RM}$ compared to T$_{CM}$ and T$_{EM}$ cells were identified with a fold change >1.5 and an expression value >120 (Fig. 1a). Genes with >1.5 fold change and >120 expression value between day 7 spleen, day 7 IELs, and day 7 kidney samples were identified (1,838 probes) and evaluated in day 7 and day 35 subsets, which were ordered with Pearson correlation using the HierarchicalClustering module of GenePattern (Fig. 1b); data were row centred, row normalized, and visualized with the HierarchicalClusteringViewer module in GenePattern.

The core tissue-residency cells and circulating signatures were generated by integrating differential expression (>1.5 fold change) data comparing T$_{RM}$ cells from the following tissues to circulating splenic memory cells (or splenic T$_{CM}$ if both T$_{CM}$ and T$_{EM}$ datasets were available): day 35 IELs (LCMV), day 35 kidney parenchyma (LCMV), day 30 skin CD103$^+$CD8$^+$ (herpes simplex virus)[5], day 30 lung CD103$^+$CD8$^+$ (influenza virus)[5], and day 20 CD103$^+$ brain (vesicular stomatitis virus)[7]; overlapping genes upregulated in all T$_{RM}$ cell populations comprised the core tissue-residency signature (121 genes) and genes downregulated in all populations comprised the circulating signature (93 genes). The mouse TIL microarray datasets were generated previously[27].

For RNA-seq analysis of day 7 IEL, day 7 memory precursors, and day 7 terminal effectors, the populations were sorted on day 7 of LCMV Armstrong infection as well as naive P14 cells; spleens or IEL samples from 2–3 mice were pooled and 5×10^3 cells were sorted. For RNA-seq analysis of TIL, congenically distinct P14 cells were transduced with Runx3-RV or GFP-RV, mixed 1:1 and 1×10^6 cells were transferred to mice with day 7 established melanoma B16-GP$_{33}$ tumours. Eight days later, 1×10^3 transduced TILs or splenocytes were sorted from four mice for each replicate. For library preparation, isolation of polyA$^+$ RNA was performed as detailed online (http://www.immgen.com/Protocols/11cells.pdf). For RNA-seq analyses of *Runx3*-manipulated cells, CD8$^+$ T cells from naive *Runx3*$^{+/+}$ YFP$^+$ (wild type) and *Runx3*$^{fl/fl}$ YFP$^+$ (*Runx3*$^{fl/fl}$) mice were enriched by negative isolation and transduced (as detailed above) with a Cre cDNA-expressing retrovirus (Cre-RV). Runx3-overexpressing cells were generated similarly by transducing *Runx3*$^{+/+}$ YFP$^+$ CD8 T cells with a *Runx3* cDNA-expressing retrovirus (Runx3-RV). Forty-eight hours after T cell receptor activation, the CD8$^+$ T cells were resuspended and re-cultured in fresh medium supplemented with 100 U ml^{-1} rhIL-2; 24 h later, YFP$^+$ (wild type or *Runx3*$^{fl/fl}$) or GFP$^+$ (Runx3-RV) were FACS-purified and then recultured in 100 U ml^{-1} IL-2. The cells were expanded until day 6 by reculturing at 5×10^5 cells per millilitre every 24 h in fresh 100 U ml^{-1} IL-2 medium. On day 6 after activation, cells were collected and total RNA was extracted in TRIzol. Purified RNA was depleted of ribosomal RNA and strand-specific paired-end libraries were prepared and sequenced using an Illumina Nextseq 500. Samples were generated from two biological replicates, and approximately 20 million paired-reads were generated per sample. Reads were mapped using Tophat[36] and aligned reads in transcripts were counted with HTseq[37]. GSEA was performed by using the GSEA module in GenePattern, and the normalized enrichment scores and false-discovery rate *q* values were determined by using the permutation test.

ATAC–seq was performed as described in detail previously[24]. Sorted cells (2.5×10^4) were resuspended in 25 μl of lysis buffer and spun down 600*g* for 30 min at 4 °C. The nuclear pellet was resuspended in 25 μl of Tn5 transposase reaction mixture (Nextera DNA Sample Prep Kit, Illumina) and incubated for 30 min at 37 °C. Transposase-associated DNA was subsequently purified (Zymo DNA clean-up kit). For library amplification, DNA was amplified using indexing primer from Nextera kit and NEBNext High-Fidelity 2× PCR master mix. Then, the amplified DNA was size-selected to fragments less than 800 bp using SPRI beads. The library was sequenced using Hiseq 2500 for single-end 50-bp sequencing to yield at least 10 million reads. We used bowtie to map raw reads to the *Mus musculus* genome (mm10) with following parameters: '–best -m 1'. We called peaks for each individual replicate as well as the pooled data from the two replicates using MACS2 with a relaxed threshold ($P = 0.01$).

For the single-cell RNA-seq analysis of human[30] and mouse melanoma TILs[29], the pre-processed single-cell TIL gene expression data were downloaded from GEO database with accessions GSE72056 or GSE86042, respectively. Activated CD8$^+$ TILs (CD8α expression > 5 and CD44 expression >2) were used and classified into *Runx3*^{hi} TILs, which express relatively high levels of *Runx3* (*Runx3* expression > 3) and *Runx3*^{lo} TILs with no *Runx3* expression (*Runx3* expression = 0). For the human TILs, melanoma #75 was used. GSEA was performed to evaluate enrichment of the core tissue-residency gene expression signature in *Runx3*^{hi} TILs relative to *Runx3*^{lo} TILs.

Computational screen: transcription factor regulatory networks and personalized PageRank analysis. Transcription factor regulatory networks and PageRank analysis were performed as described previously[24] except that gene expression and ATAC–seq data from day 7 IEL, kidney and spleen samples were used. To construct the transcription factor regulatory network, transcription factor-binding motifs were first scanned on ATAC–seq peaks using an algorithm described previously[14] and a *P*-value cut-off of 1×10^{-5}. Then, we connected a transcription factor to a gene if the factor had any predicted binding motif in the ATAC–seq peak of the nearest gene. We assembled all the interactions between transcription factors and genes into a regulatory network. To identify important transcription factor regulators for T$_{RM}$ cell differentiation, we performed personalized PageRank analysis in the transcription factor regulatory network constructed above using the pipeline described previously[14]. The importance of a transcription factor is based on the quantity and quality of its regulated gene targets. A factor would receive a higher PageRank score if it regulates more important genes, where the importance is evaluated by differential expression from microarray or RNA-seq analyses. Extended Data Fig. 2b and Supplementary Table 1 indicate the PageRank score and expression value of all transcription factors expressed (>120 expression value) in the spleen, kidney or IEL cells.

Statistical analysis. Student's *t*-test (two-tailed) was used for comparisons between two groups. A log-rank (Mantel–Cox) test was used to compare survival curves. All microarray, RNA-seq, and ATAC–seq samples were performed independently in

2–3 replicates. All statistical tests were performed with GraphPad Prism software, and $P < 0.05$ was considered statistically significant. No statistical methods were used to predetermine sample size. Investigators were not blinded to allocation during experiments and outcome assessment.

Data availability. RNA-seq, microarray, and ATAC–seq data are available in the Gene Expression Omnibus (GEO) database under the SuperSeries reference code GSE107395. Source Data are provided in the online version of the manuscript. All other data are available from the corresponding author(s) upon reasonable request.

31. Steinert, E. M. *et al.* Quantifying memory CD8 T cells reveals regionalization of immunosurveillance. *Cell* **161,** 737–749 (2015).
32. Benck, C. J., Martinov, T., Fife, B. T. & Chatterjea, D. Isolation of infiltrating leukocytes from mouse skin using enzymatic digest and gradient separation. *J. Vis. Exp.* **107,** e53638 (2016).
33. Knott, S. R. V. *et al.* A computational algorithm to predict shRNA potency. *Mol. Cell* **56,** 796–807 (2014).
34. Pear, W. S. *et al.* Efficient and rapid induction of a chronic myelogenous leukemia-like myeloproliferative disease in mice receiving P210 bcr/abl-transduced bone marrow. *Blood* **92,** 3780–3792 (1998).
35. Best, J. A. *et al.* Transcriptional insights into the $CD8^+$ T cell response to infection and memory T cell formation. *Nat. Immunol.* **14,** 404–412 (2013).
36. Trapnell, C., Pachter, L. & Salzberg, S. L. TopHat: discovering splice junctions with RNA-Seq. *Bioinformatics* **25,** 1105–1111 (2009).
37. Anders, S., Pyl, P. T. & Huber, W. HTSeq—a Python framework to work with high-throughput sequencing data. *Bioinformatics* **31,** 166–169 (2015).

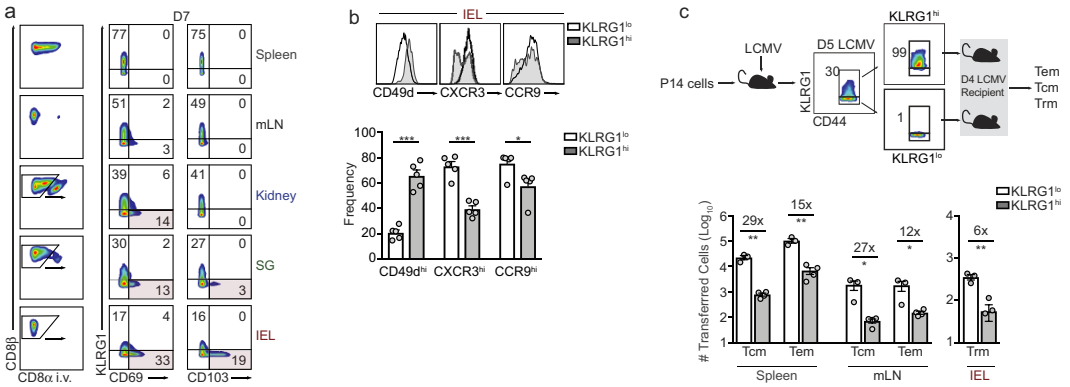

Extended Data Figure 1 | KLRG1^{lo} cells preferentially give rise to T_{RM} cells. a, Left, representative flow cytometric gating strategy for distinguishing P14 cells located in non-lymphoid tissues after intravenous administration of CD8α in LCMV-infected mice. Right, *in vitro* activated P14 cells were transferred to recipient mice and infected with LCMV; the frequency of CD69^{+} and CD103^{+} P14 cells among KLRG1^{hi} and KLRG1^{lo} on day 7 of infection is indicated. **b**, Frequency of CCR9, CXCR3 and CD49d in KLRG1^{lo} and KLRG1^{hi} cells in the IEL compartment on day 7 of infection. **c**, Top, schematic of experimental design. KLRG1^{lo} and KLRG1^{hi} P14 cells were sorted from spleens and lymph nodes on day 5 of LCMV infection and transferred into recipient mice infected 4 days previously with LCMV. Bottom, T_{CM}, T_{EM} and T_{RM} P14 cells were enumerated on days 20 or 25 of infection using flow cytometry. Data are mean ± s.e.m of $n = 5$ mice (**a**, **b**) or $n = 3$–4 mice (**c**) from one representative of 2 independent experiments. $^{*}P < 0.05$, $^{**}P < 0.01$, $^{***}P < 0.005$ (Student's *t*-test). Symbols represent an individual mouse (**c**).

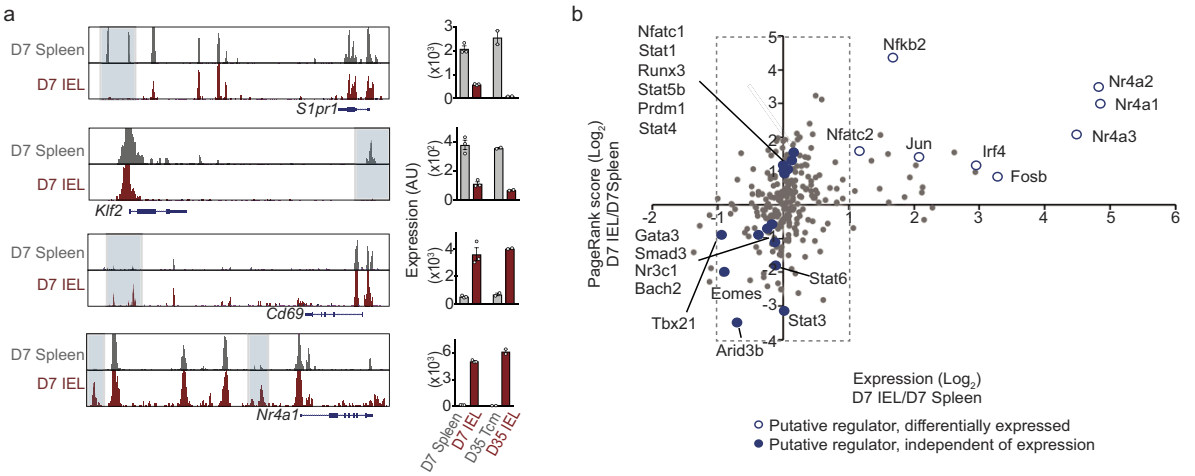

Extended Data Figure 2 | Representative ATAC–seq peaks and putative T_{RM} cell regulators identified through PageRank analysis. a, ATAC–seq analysis of the indicated loci on day 7 of infection (left) and corresponding gene expression (right). **b**, Personalized PageRank score and gene expression of transcription factors, with selected factors highlighted.

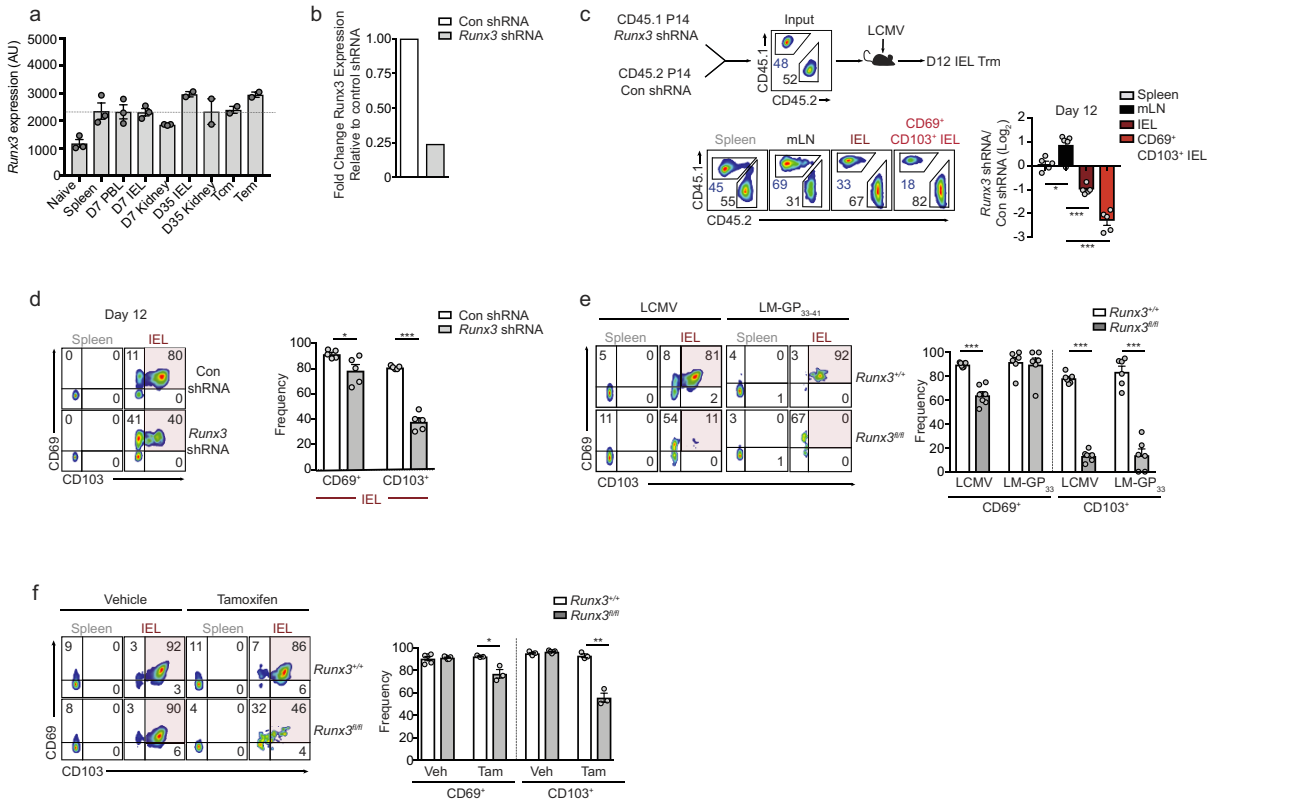

Extended Data Figure 3 | *Runx3*-deficiency impairs IEL T_{RM} cell formation. a, *Runx3* mRNA levels from indicated cells determined by microarray analyses. **b**, Relative *Runx3* mRNA expression of *in vitro* cultured cells transduced with retroviruses encoding control shRNAmir or *Runx3* shRNAmir, measured by qPCR. **c**, Congenically distinct P14 cells were transduced with retroviruses encoding *Runx3* shRNAmir or control shRNAmir, mixed at a 1:1 ratio, and transferred to recipient mice that were subsequently infected with LCMV. Representative flow cytometry plots (bottom, left) and quantification of the ratio of P14 cells transduced with *Runx3* shRNAmir or control shRNAmir in indicated tissues on day 12 of infection (bottom, right). **d**, Representative flow cytometry plots (left) and quantification of the frequency of $CD69^+$ and $CD103^+$ cells of control shRNAmir or *Runx3* shRNAmir cells (right) from experimental schematic in **c**. **e**, Representative flow cytometry plots and quantification of the frequency of $CD69^+$ and $CD103^+$ cells from Fig. 2c. **f**, Representative flow cytometry plots and quantification of the frequency of $CD69^+$ and $CD103^+$ cells from Fig. 2e. Data are mean ± s.e.m and representative of two independent experiments (**b**) with $n = 5$ (**c**, **d**), $n = 5$ (LM–$GP_{33–41}$) or $n = 6$ (LCMV) (**e**), and $n = 5$ (vehicle) or $n = 3$ (tamoxifen) (**f**). $^*P < 0.05$, $^{**}P < 0.01$ $^{***}P < 0.005$ (Student's *t*-test). Symbols represent an individual mouse (**c**–**f**).

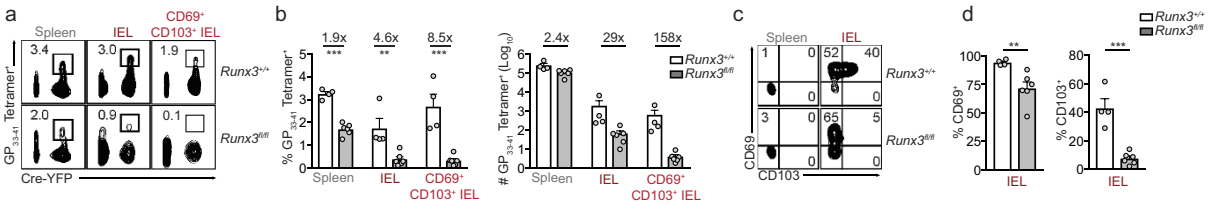

Extended Data Figure 4 | *Runx3*-deficiency impairs IEL T_{RM} cell formation in a polyclonal setting. a, Representative flow cytometry plot of H-2D^b $GP_{33–41}$ tetramer staining of lymphocytes from *Runx3*$^{fl/fl}$ dLck-Cre$^+$YFP and Runx3$^{+/+}$dLck-Cre$^+$YFP mice on day 12 of LCMV infection (gated on total lymphocytes). **b**, Quantification of the proportion (left) and absolute number (right) of tetramer$^+$ cells. **c**, **d**, Representative flow cytometry plots and quantification of the frequency of CD69$^+$ and CD103$^+$ cells. Data are mean ± s.e.m with $n = 4$ (*Runx3*$^{+/+}$) or $n = 5$ (*Runx3*$^{fl/fl}$) mice pooled from two independent experiments. $^{**}P < 0.01$, $^{***}P < 0.005$ (Student's *t*-test). Symbols represent an individual mouse (**b**, **d**).

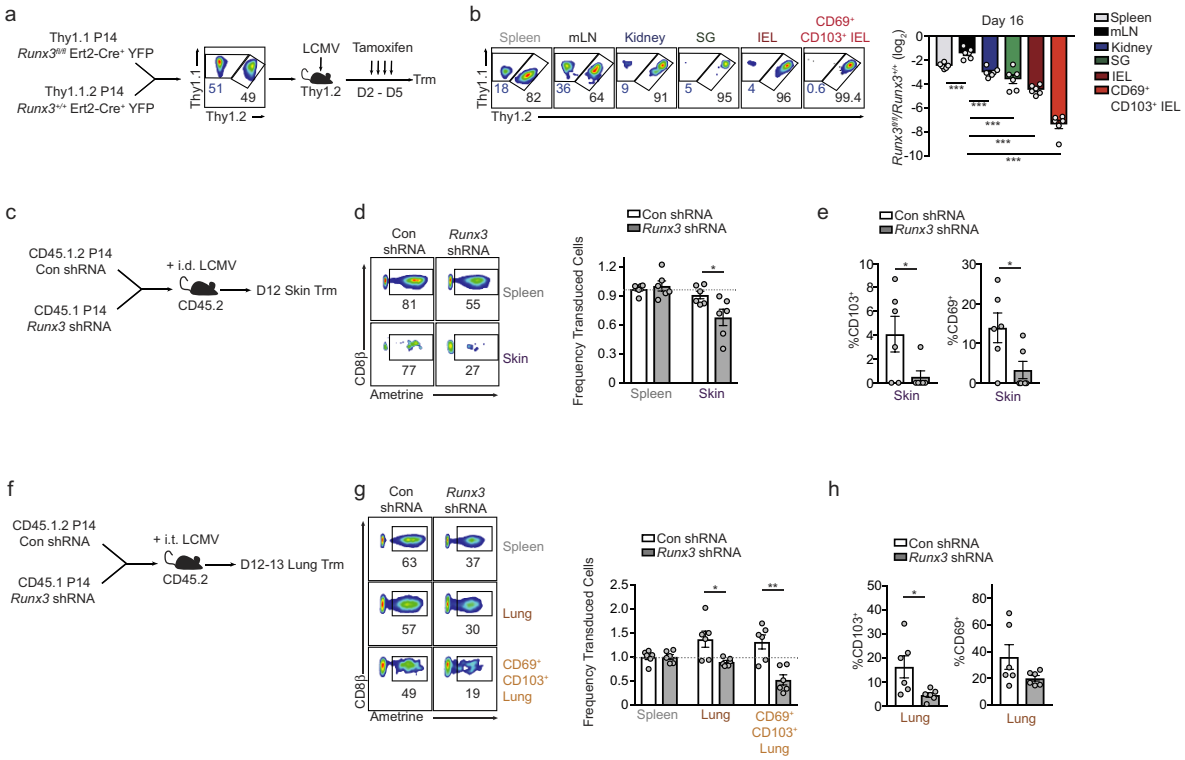

Extended Data Figure 5 | Runx3 is required for T_{RM} cell formation in diverse non-lymphoid tissues. a, Schematic of experimental design. **b**, Representative flow cytometry plots (left) and quantification (right) of the ratio of *Runx3*$^{fl/fl}$ to *Runx3*$^{+/+}$ P14 cells (gated on YFP-Cre^{+} cells) in lymphoid and non-lymphoid compartments on days 15/16 of LCMV infection (as in Fig. 2d but including salivary gland (SG) and kidney populations). **c**, Schematic for experimental design. **d**, Representative flow cytometry plots (left) and quantification (right) of the ratio of transduced cells in the skin relative to the spleen for control shRNAmir or *Runx3* shRNAmir P14 cells on day 12 of an intradermal LCMV infection. **e**, Frequency of CD69^{+} and CD103^{+} cells. **f**, Schematic for experimental design. **g**, Representative flow cytometry plots (left) and quantification (right) of the ratio of transduced cells in the lung parenchyma relative to the spleen for control shRNAmir or *Runx3* shRNAmir P14 cells on day 12 of an intratracheal LCMV infection. **h**, Frequency of CD69^{+} and CD103^{+} cells. Data are mean ± s.e.m and representative of two independent experiments with $n = 6$ (**b**), or data pooled from two individual experiments with $n = 6$ per group (**c**–**h**). $^{*}P < 0.05$, $^{**}P < 0.01$, $^{***}P < 0.005$ (Student's *t*-test). Symbols represent an individual mouse (**b**, **d**, **e**, **g**, **h**).

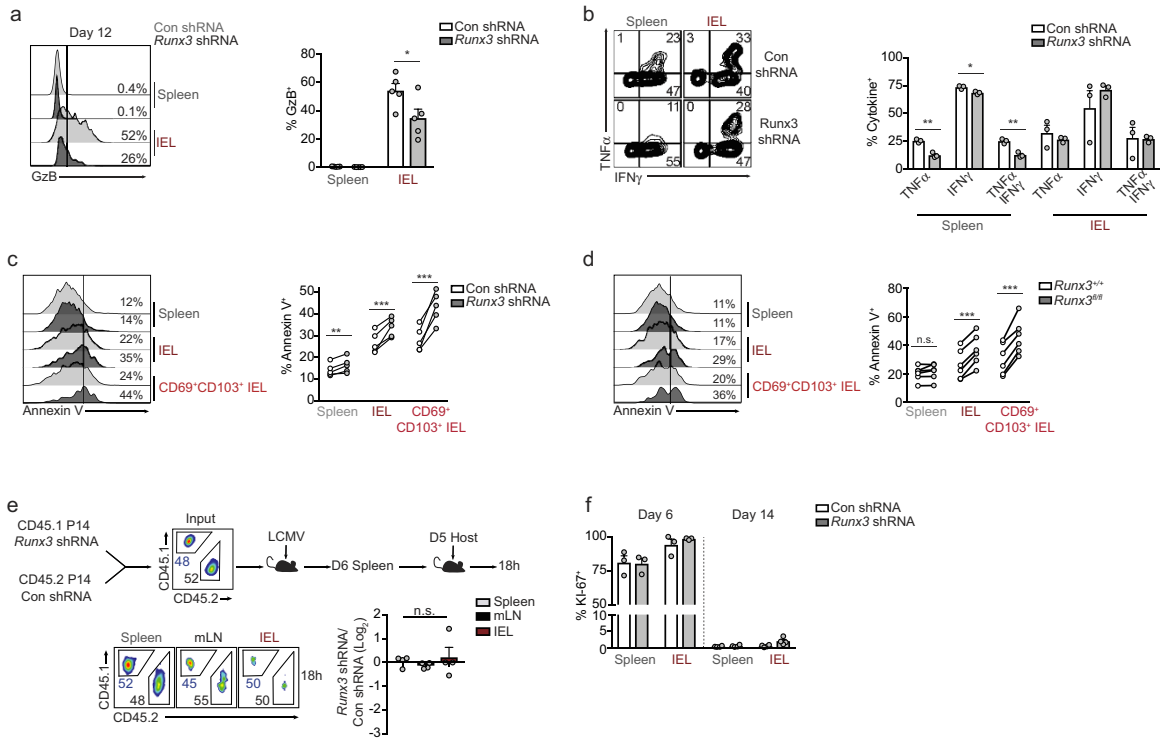

Extended Data Figure 6 | *Runx3*-deficiency enhances T_{RM} cell apoptosis but does affect trafficking or proliferation. a, Representative flow cytometry histogram of granzyme B (GzB) staining (left) and quantification of frequency of GzB^+ cells on day 12 or 14 of infection. **b**, Representative flow cytometry plots (left) and quantification (right) of the frequency of IFNγ- and TNF-producing control shRNAmir or *Runx3* shRNAmir P14 cells on day 6 of LCMV infection, restimulated with $GP_{33–41}$ peptide. **c**, **d**, Representative histograms and quantification of annexin V^+ cells from shRNAmir mixed transfers on day 14 of LCMV infection (**c**) or from day 8 $Runx3^{fl/fl}$ and $Runx3^{+/+}$ mixed P14 transfers in which tamoxifen was administered on days 2–5 of LCMV infection (**d**). **e**, Congenically distinct P14 cells were transduced with control shRNAmir or *Runx3* shRNAmir encoding retroviruses, mixed at a 1:1 ratio, and transferred to recipient mice that were subsequently infected with LCMV. On day 6 of infection, splenocytes were collected and retransferred to day 5 infected host mice and 18 h later spleen, mesenteric lymph nodes and small intestine were obtained to assess trafficking. Representative flow cytometry plots (bottom, left) and quantification of the ratio of P14 cells transduced with control shRNAmir to *Runx3* shRNAmir (bottom, right) in indicated tissues 18 h after transfer. **f**, Frequency of Ki-67^+ control shRNAmir or *Runx3* shRNAmir transduced P14 cells in a mixed transfer setting on days 6 and 12 or 14 of LCMV infection. Data are mean ± s.e.m and representative of two independent experiments with $n = 5$ (**a**), $n = 3$ (**b**), $n = 5$ (**c**), $n = 6$ (**d**), $n = 4$ (**e**), and $n = 3$ on day 6 or $n = 4$ on day 14 (**f**) except **d** is pooled from two independent experiments. $^*P < 0.05$, $^{**}P < 0.01$, $^{***}P < 0.005$ (Student's *t*-test). n.s., not significant. Symbols represent an individual mouse (**a**–**f**).

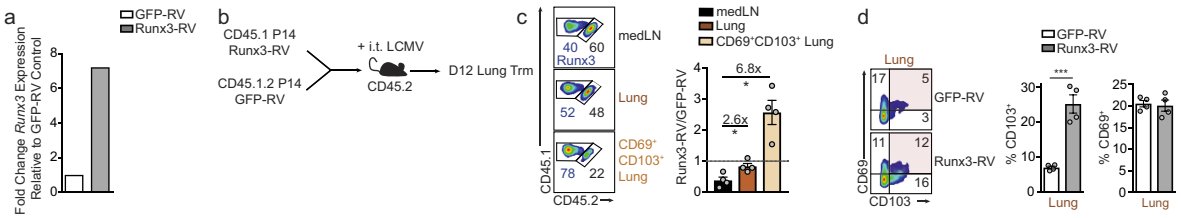

Extended Data Figure 7 | Runx3 overexpression enhances lung T_{RM} differentiation. a, *Runx3* mRNA expression of *in vitro* cultured cells transduced with GFP-RV or Runx3-RV. **b**, Schematic for experimental design of intratracheal LCMV infection. **c**, Representative flow cytometry plots (left) and quantification (right) of the ratio of GFP-RV or Runx3-RV cells in the mediastinal lymph nodes (medLN), lung parenchyma, or $CD69^+CD103^+$ lung parenchyma population on day 12 or 13. **d**, Representative flow cytometry plots (left) and quantification (right) of the frequency of $CD69^+$ and $CD103^+$ P14 cells in the lung parenchyma. Data are mean ± s.e.m and representative of one of two independent experiments (**a**) and $n = 4$ per group (**c**,**d**). $^*P < 0.05$, $^{***}P < 0.005$ (Student's *t*-test). Symbols represent an individual mouse (**c**, **d**).

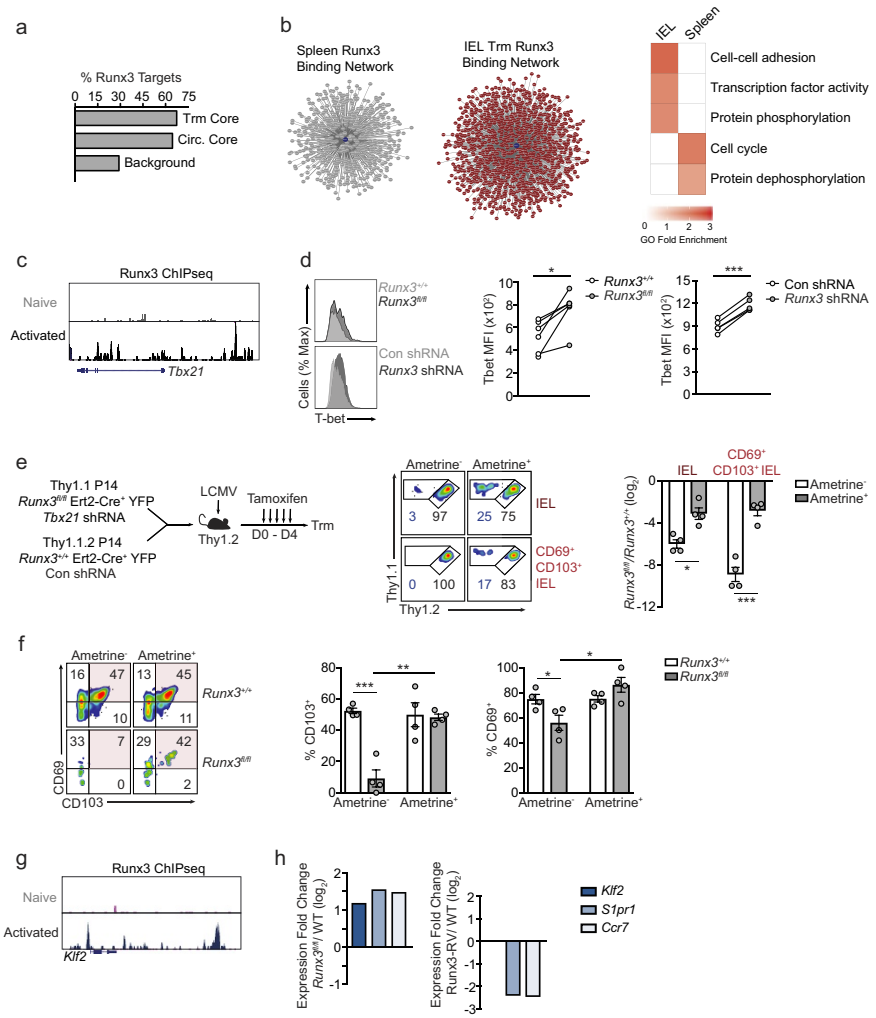

Extended Data Figure 8 | Runx3 regulates distinct gene programs in circulating cells versus tissue resident cells and operates upstream of T-bet in programming IEL T_{RM} cell differentiation. a, Percentage of genes of the core tissue-residency signature, core circulating signature, or background sites that exhibit direct Runx3 binding by ChIP–seq analysis[23]. **b**, Left, predicted Runx3 binding network, generated from ATAC–seq analysis, in IEL P14 cells and splenic P14 cells on day 7 of infection. Red indicates genes putatively regulated by Runx3 in IEL cells; grey indicates genes putatively regulated by Runx3 in splenic cells. Right, Gene Ontology (GO) enrichment analysis of gene sets in the predicted Runx3 binding network in each tissue. **c**, Runx3 ChIP–seq of the *Tbx21* locus in naive and activated $CD8^+$ T cells from ref. 23. **d**, Representative flow cytometry histograms (left) and mean fluorescent intensity (MFI) quantification (right) of T-bet expression in splenic P14 cells on day 8 of infection. **e**, Schematic for experimental design (left) in which *Runx3*$^{+/+}$ Ert2-Cre^+ YFP were transduced with control shRNAmir and *Runx3*$^{+/+}$ Ert2-Cre^+ YFP P14 cells were transduced with *Tbx21* shRNAmir, mixed 1:1 and transferred into recipient mice subsequently infected with LCMV. Recipient mice were treated with tamoxifen on days 0–4 of infection. Representative flow cytometry plots (middle) and quantification of the ratio of untransduced (ametrine$^-$) *Runx3*$^{+/+}$ and *Runx3*$^{fl/fl}$ P14 cells and the ratio of transduced (ametrine$^+$) *Runx3*$^{+/+}$ control shRNAmir to *Runx3*$^{fl/fl}$ *Tbx21* shRNAmir (right) were evaluated on day 12 of LCMV infection. **f**, Representative flow cytometry plots (left) and quantification (right) of the frequency of $CD69^+$ and $CD103^+$ cells. **g**, Runx3 ChIP–seq of the *Klf2* locus in naive and activated $CD8^+$ T cells[23]. **h**, Fold change in gene expression of *Klf2*, *S1pr1* and *Ccr7* in *Runx3*$^{fl/fl}$ and Runx3-RV cells relative to *Runx3*$^{+/+}$ wild-type cells, from RNA-seq analysis consisting of two replicates per sample. Data are mean ± s.e.m and representative of one of two independent experiments with $n = 6$ (*Runx3*$^{fl/fl}$) or $n = 4$ (*Runx3* shRNAmir) (**d**) and $n = 4$ (**e**, **f**) per group. $^*P < 0.05$, $^{**}P < 0.01$ $^{***}P < 0.005$ (Student's *t*-test). Symbols represent an individual mouse (**d**–**f**).

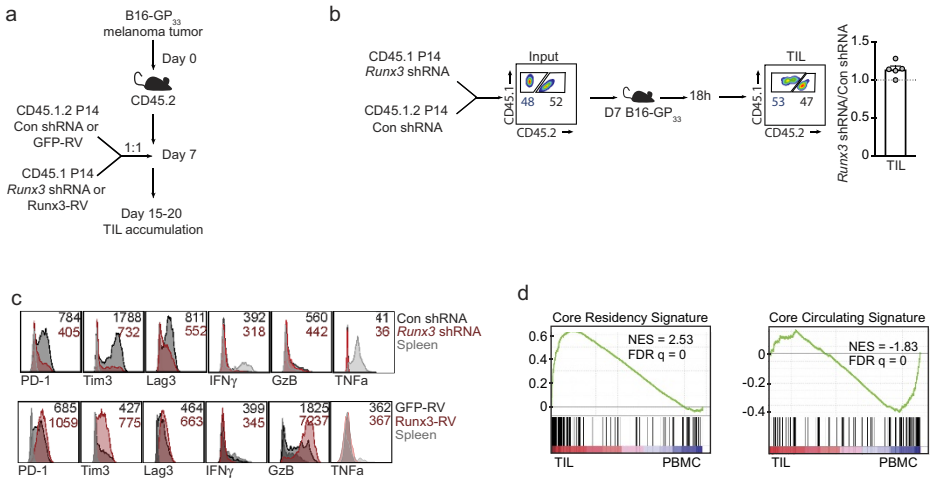

Extended Data Figure 9 | *Runx3*-deficiency does not impair trafficking to the tumour but does affect the effector phenotype of TIL. a, Schematic of adoptive therapy experimental design. **b**, Congenically distinct P14 cells were transduced with retroviruses encoding *Runx3* shRNAmir or control shRNAmir, mixed at a 1:1 ratio, and transferred into mice with established B16-GP_{33} melanoma tumours. Eighteen hours after transfer, tumours were collected to assess the ratio of *Runx3* shRNAmir to control shRNAmir P14 cells. **c**, Representative flow cytometry histograms of control shRNAmir, *Runx3* shRNAmir, GFP-RV, or Runx3-RV TILs in mixed transfer settings. Control P14 splenocytes were included in histograms for reference. **d**, Gene set enrichment analysis of the core tissue-residency and core circulating gene signatures in human lung $CD8^+$ TILs relative to corresponding $CD8^+$ PBMCs[25]. Data are mean ± s.e.m and combined of two independent experiments with $n = 5$ mice per group (**b**) or representative of two independent experiments with $n = 3–6$ per group (**b**). Symbols represent an individual mouse (**b**).

nature research

Corresponding author(s): Goldrath, A.G.

☐ Initial submission ☐ Revised version ☒ Final submission

Life Sciences Reporting Summary

Nature Research wishes to improve the reproducibility of the work that we publish. This form is intended for publication with all accepted life science papers and provides structure for consistency and transparency in reporting. Every life science submission will use this form; some list items might not apply to an individual manuscript, but all fields must be completed for clarity.

For further information on the points included in this form, see Reporting Life Sciences Research. For further information on Nature Research policies, including our data availability policy, see Authors & Referees and the Editorial Policy Checklist.

Experimental design

1. Sample size

Describe how sample size was determined.

Based on previous and preliminary studies within our lab, we predicted the reported sample sizes would be sufficient to ensure adequate power. For Figures 2 and 3, we expected to see a 50-75% difference in Runx3-deficient Trm compared with control Trm cells in shRNA and KO models or Runx3-RV compared to GFP-RV cells; therefore, a sample size of n=3-8 was chosen to allow determination of at least a 50% reduction in Trm (t-test, α set at 0.05). For Figure 4 d,e we also expected to see 50-75% difference in Runx3 shRNA TIL compared with control shRNA TIL or Runx3-RV compared to GFP-RV TIL; therefore, a sample size of n=3-7 was chosen to allow determination of at least a 50% reduction in TIL accumulation (t-test, α set at 0.05). For Figure 4 g,h, we expected to see a 20-50% difference in tumor size and mortality between Runx3 shRNA and control shRNA groups or Runx3-RV and GFP-RV groups; therefore, a sample size of 10-21 was chosen (t-test, α set at 0.05 or Log-rank test). Figure 1 sample sizes were chosen to achieve a sufficient cell number after sorting for subsequent processing, based on previous experiments within the lab.

2. Data exclusions

Describe any data exclusions.

No data were excluded from analyses except in adoptive transfer/LCMV infection experiments, recipient mice that rejected transferred P14 cells (<~5%) were excluded (Figures 2-3).

3. Replication

Describe whether the experimental findings were reliably reproduced.

All attempts at replication were successful.

4. Randomization

Describe how samples/organisms/participants were allocated into experimental groups.

Mice were chosen at random for each group prior to all adoptive cell transfers and all tumor transplants.

5. Blinding

Describe whether the investigators were blinded to group allocation during data collection and/or analysis.

For all mixed transfer experiments, blinding is not relevant. For tumor growth assessments, the investigator was aware of the cell type the was transferred into tumor-bearing mice.

Note: all studies involving animals and/or human research participants must disclose whether blinding and randomization were used.

6. Statistical parameters

For all figures and tables that use statistical methods, confirm that the following items are present in relevant figure legends (or in the Methods section if additional space is needed).

n/a	Confirmed
☐	☒ The exact sample size (*n*) for each experimental group/condition, given as a discrete number and unit of measurement (animals, litters, cultures, etc.)
☐	☒ A description of how samples were collected, noting whether measurements were taken from distinct samples or whether the same sample was measured repeatedly
☐	☒ A statement indicating how many times each experiment was replicated
☐	☒ The statistical test(s) used and whether they are one- or two-sided (note: only common tests should be described solely by name; more complex techniques should be described in the Methods section)
☐	☒ A description of any assumptions or corrections, such as an adjustment for multiple comparisons
☐	☒ The test results (e.g. *P* values) given as exact values whenever possible and with confidence intervals noted
☐	☒ A clear description of statistics including central tendency (e.g. median, mean) and variation (e.g. standard deviation, interquartile range)
☐	☒ Clearly defined error bars

See the web collection on statistics for biologists for further resources and guidance.

Software

Policy information about availability of computer code

7. Software

Describe the software used to analyze the data in this study.	The PageRank analysis utilized in Figure 1 was described in detail previously (Yu et al., Nat. Immunol, 2017).

For manuscripts utilizing custom algorithms or software that are central to the paper but not yet described in the published literature, software must be made available to editors and reviewers upon request. We strongly encourage code deposition in a community repository (e.g. GitHub). *Nature Methods* guidance for providing algorithms and software for publication provides further information on this topic.

Materials and reagents

Policy information about availability of materials

8. Materials availability

Indicate whether there are restrictions on availability of unique materials or if these materials are only available for distribution by a for-profit company.	All unique materials used are readily available from the authors.

9. Antibodies

Describe the antibodies used and how they were validated for use in the system under study (i.e. assay and species).

The antibodies are described below. All antibodies were purchased from eBioscience unless specified. All antibodies were validated by manufacturer.

Antibody Clone Color Catalog # Lot #

CD8a 53-6.7 eFluor780 470081-82 4322567

CD8b eBio H35-17.2 BV421 (eFluor450) 480083-82 E16107-105
CD8b eBio H35-17.2 PE 12-0083-82 4287758

CD62L MEL-14 BV510 (BioLegend) 104441 B213054
CD62L MEL-14 PE-Cy7 25-0621-82 4277103
CD62L MEL-14 Fitc 11-0621-82 4278965

CD127 A7R34 PE-Cy7 25-1271-82 E07599-1635

KLRG1 2F1 PB (eFluor450) 48-5893-82 4271587
KLRG1 2F1 APC 17-5893-82 4323183

CD103 2E7 Fitc 11-1031-85 E00455-1634
CD103 2E7 PE 12-1031-83 4303133
CD103 2E7 Percp Cy5.5 (BioLegend) 121412 B212948

CD69 H1.2F3 Percp Cy5.5 45-0691-82 4313339
CD69 H1.2F3 BV711 (BioLegend) 104537 B240847

CD45.1 A20-1.7 BV785 (BioLegend) 110743 B231586
CD45.1 A20-1.7 PB (eFluor450) 480453-82 4313590

CD45.2 104 APC 17-0454-82 4290825
CD45.2 104 Percp Cy5.5 45-0454-82 4277873

Thy1.1 OX-7 PB (BioLegend) 202529 B231585
Thy1.1 OX-7 PE-Cy7 250900-82 E07586-1633

Thy1.2 53-2.1 APC 17-0902-82 E07187-1635
Thy1.2 30-H12 BV785 (BioLegend) 105331 B229101

CCR9 eBio CW-1.2 PE-Cy7 25-1991-82 4278641

CXCR3 CXCR3-173 PE 12-1831-82 4299803

CD49d R1-2 Fitc 11-0492-85 E003441630

T-bet 4B10 PE-Cy7 (BioLegend) 644823 B214293

TNFa MP6-XT22 APC 17-7321-82 E07384-1631

GzB GB11 PE MHGB04 1850394
GzB GB11 APC MHGB05 1884625

PD-1 J43 APC-Cy7 47-9985-82 4324436

Tim3 RMT3-23 PE 12-5870-82 E01844-1634

Lag3 eBio C9B7N Percp Cy5.5 46-2231-82 4295768

KI-67 SolA15 PB (eFluor450) 48-5698-82 4297555

10. Eukaryotic cell lines

a. State the source of each eukaryotic cell line used.

B16 mouse melanoma cells expressing B16gp33-41 were used, and were gifted by Alain Lamarre (INRS).

b. Describe the method of cell line authentication used.

B16-GP33 has been authenticated in our lab, as they form melanoma tumors and using P14 T cells in killing assays to confirm GP33 expression..

c. Report whether the cell lines were tested for mycoplasma contamination.

B16-GP33 cells were treated for mycoplasma contamination prior to use.

d. If any of the cell lines used are listed in the database of commonly misidentified cell lines maintained by ICLAC, provide a scientific rationale for their use.

No commonly misidentified cell lines were used.

Animals and human research participants

Policy information about studies involving animals; when reporting animal research, follow the ARRIVE guidelines

11. Description of research animals

Provide details on animals and/or animal-derived materials used in the study.

All mice were of a C57BL6/J background and bred at UCSD and TSRI-FL or purchased from the Jackson Laboratory, including: WT or P14 mice with distinct expression of the congenic molecules CD45.1, CD45.1.2, CD45.2, Thy1.1, Thy1.1.2, and Thy1.2 as well as control Thy1.2+ Runx3+/+Ert2-Cre+YFP P14 mice and Runx3 inducible deletion Thy1.1+Runx3fl/flErt2-Cre+YFP P14 mice. Runx3+/+dLck-Cre+YFP and Runx3fl/fldLck-Cre+YFP mice were used for studying polyclonal CD8+ T cell responses. The Rosa26 stop-flox eYFP reporter mice were used for all Runx3-deletion experiments. Both male and female mice were used, and all mice were used at 6-20 wks of age.

Policy information about studies involving human research participants

12. Description of human research participants

Describe the covariate-relevant population characteristics of the human research participants.

The study did not involve human research participants.

nature research

Corresponding author(s): Goldrath, A.W.

☐ Initial submission ☐ Revised version ☒ Final submission

Flow Cytometry Reporting Summary

Form fields will expand as needed. Please do not leave fields blank.

Data presentation

For all flow cytometry data, confirm that:

☒ 1. The axis labels state the marker and fluorochrome used (e.g. CD4-FITC).

☒ 2. The axis scales are clearly visible. Include numbers along axes only for bottom left plot of group (a 'group' is an analysis of identical markers).

☒ 3. All plots are contour plots with outliers or pseudocolor plots.

☒ 4. A numerical value for number of cells or percentage (with statistics) is provided.

Methodological details

5. Describe the sample preparation.	For isolation of CD8+ T cells from the small intestine intraepithelial lymphocyte (IEL) compartment, Peyer's patches were removed and the intestine was cut longitudinally and subsequently cut laterally into 0.5-1cm2 pieces that were then incubated with 0.154mg/mL dithioerythritol (DTE) in 10% HBSS/HEPES bicarbonate for 30min at 37°C while stirring. Kidneys, salivary glands and lungs were cut into pieces and digested for 30min with 100 U/mL type I collagenase (Worthington) in RPMI 1640, 5% FBS, 2mM MgCl2, 2mM CaCl2 at 37°C while shaking. Skin was processed similarly as described (ref 50) in which a 2cm2 area of the right flank was excised, pre-digested for 30min at 37°C and then enzymatically digested with 0.7 mg/mL collagenase D. After enzymatic incubations (skin, lungs, kidneys, salivary glands), tissues were further dissociated over a 70µm nylon cell strainer (Falcon). For isolation of lymphocytes, single-cell suspensions were then separated using a 44/67% Percoll density gradient. Spleens and lymph nodes were processed with the frosted ends of microscope slides. Red blood cells were lysed with ACK buffer (140 mM NH4Cl and 17 mM Tris-base, pH 7.4).
6. Identify the instrument used for data collection.	For flow cytometry analysis, all events were acquired on a BD LSRFortessa X-20 or a BD LSRFortessa.
7. Describe the software used to collect and analyze the flow cytometry data.	The software used for collecting was BDFACS Diva software and for analyzing FlowJo software was used.
8. Describe the abundance of the relevant cell populations within post-sort fractions.	The purity of sorted samples were typically >98% pure. To check purity, an aliquot of sorted cells was analyzed or in cases where cells were sorted directly into Trizol, an additional aliquot of cells were sorted and purity was checked.
9. Describe the gating strategy used.	For all analyses, gating schematics consisted of FSCxSSC gating of lymphocytes followed by singlet discrimination gates. For Figure 1, all sorted cells from the mLN, spleen or blood were sorted based on CD8a+ and congenic markers followed by CD127, KLRG1 or CD62l as indicated. For IEL or kidney populations CD8a IV negative CD8b+ cells were gated on and congenic markers were used for sorting. For Figure 2 and 3, CD8a+ cells were gated on, then ametrine (shRNA

experiments) or YFP (knockout experiments) then congenic markers (CD45.1, CD45.2, CD45.1.2, Thy1.1, Thy1.1.2 or Thy1.2) were gated on to distinguish mixed populations. Subsequent analysis of congenically distinct populations included expression levels of CD103, CD69, propidium iodide and Annexin V.

For Figure 3, the same gating strategy was used as in Figure 2 except transduced cells were GFP+ instead of ametrine+. Gating and sorting strategy for Fig. 3 RNAseq data is discussed in Methods (p. 18).

For Figure 4, analysis of mixed transfer populations in tumors was performed as described for Figure 2. Transduced and expanded P14 cells were sorted on Ametrine or GFP reporter expression for efficacy experiments.

Tick this box to confirm that a figure exemplifying the gating strategy is provided in the Supplementary Information. ☒

ERRATUM

doi:10.1038/nature25445

Erratum: Runx3 programs CD8$^+$ T cell residency in non-lymphoid tissues and tumours

J. Justin Milner, Clara Toma, Bingfei Yu, Kai Zhang, Kyla Omilusik, Anthony T. Phan, Dapeng Wang, Adam J. Getzler, Toan Nguyen, Shane Crotty, Wei Wang, Matthew E. Pipkin & Ananda W. Goldrath

Nature **552,** 253–257 (2017); doi:10.1038/nature24993

In this Letter, owing to errors introduced during the proofreading process, the words 'infection with' were missing from the sentence "Furthermore, *Runx3* RNAi also impaired T_{RM} cell differentiation in the context of a localized infection with enteric *Listeria monocytogenes* expressing $GP_{33–41}$ (LM–$GP_{33–41}$) (Fig. 2b)." In addition, in Fig. 1a, the *x*-axis label for the bottom right graph should have read "Expression change $\log_2$(D7 kid/D7 T_{CM})" rather than "Expression change $\log_2$(D35 kid/D35 T_{CM})". In Fig. 1e, the arrow pointing from the spleen to T_{CM} should have been enlarged and aligned with the arrow above, and in the heat map in Fig. 1f '*Irf4*' should have been non-italic upright font. These errors have all been corrected in the online versions of the Letter. Supplementary Information to this Corrigendum shows the original uncorrected Fig. 1, for transparency.

Supplementary Information is available in the online version of this Corrigendum.